Bull. Astr. Soc. India (2011) **39**, 471–515

An overview of the current understanding of Gamma Ray Bursts in the Fermi era

P. N. Bhat[1]* and S. Guiriec[1,2]†

[1] *University of Alabama in Huntsville, 320 Sparkman Dr., Huntsville, AL, 35805, USA*
[2] *NASA, Goddard Space Flight Center, Greenbelt, MD 20771, USA*

Received 2011 November 07; accepted 2011 November 12

Abstract. Gamma-ray bursts are the most luminous explosions in the Universe, and their origin as well as mechanism are the focus of intense research and debate. More than three decades since their serendipitous discovery, followed by several breakthroughs from space-borne and ground-based observations, they remain one of the most interesting astrophysical phenomena yet to be completely understood. Since the launch of Fermi with its unprecedented energy band width spanning seven decades, the study of gamma-ray burst research has entered a new phase. Here we review the current theoretical understanding and observational highlights of gamma-ray burst astronomy and point out some of the potential promises of multi-wavelength observations in view of the upcoming ground based observational facilities.

Keywords : gamma-rays: bursts – gamma-rays: observations – gamma-rays: theory

1. Introduction

Gamma-ray bursts (GRBs) are short, intense and distant flashes of γ-rays that occur at random locations in the sky with their peak power in the 200–500 keV range. During their appearance, they often outshine all other sources combined in the γ-ray sky. Early observations have detected what is now referred to as the prompt emission which is brief (milliseconds to minutes), highly variable (in time scales of sub-ms to tens of seconds), non-thermal, and observed mostly in the keV/MeV energy range. A breakthrough in the field of GRB research happened with the numerous GRB detections from the Burst And Transient Source Experiment (BATSE), which flew, with other instruments, on board the Compton Gamma-Ray Observatory (CGRO). Before BATSE, the

*email: Narayana.Bhat@nasa.gov
†email: sylvain.guiriec@nasa.gov, NASA Postdoctoral Program Fellow

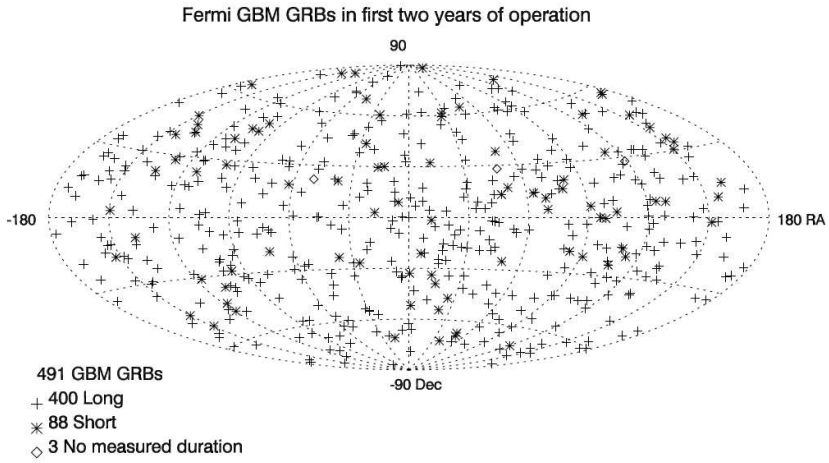

Figure 1. During the first 2 years of operation GBM detected and located 491 GRBs. The locations for 400 long bursts and 88 short bursts are plotted in this figure separately to demonstrate that the both long and short GRBs are uniformly distributed in the sky and is consistent with the earlier results of BATSE experiment underlining their cosmological origin.

distance scale of GRBs was unknown. The scientific opinion at the time was divided among the various theories predicting distance scales ranging from our own solar system to the edges of the known Universe.

BATSE's improved spatial sensitivity proved that GRBs are isotropically distributed on the celestial sphere ruling out possible correlations with the local distribution of stellar or gaseous mass (e.g. our Galaxy, the LMC, M31, globular clusters, the Virgo cluster) which is not isotropic. Fig. 1 shows a sky distribution of GRBs from the recent Gamma-ray Burst Monitor (GBM) experiment (see §4.1 for details).

This piece of evidence strongly suggested a cosmological origin for GRBs although an extended halo around our galaxy could still generate a uniform distribution similar to the one observed. Key GRB properties have emerged as soon as their cosmological nature has been established by BATSE (Fishman & Meegan 1995). GRBs have been thought as probes of the processes and environments of star formation out to the earliest cosmic epochs.

After CGRO the Russian Konus experiment (Aptekar et al. 1995) on board the Wind satellite launched in November 1994 as well as High Energy Transient Explorer (HETE-2) experiment (Ricker et al. 2003) launched in October 2000 recorded more than 2000 GRBs (Cline et al. 2003; Vanderspek et al. 2004) adding to the earlier record of more than 2700 GRBs recorded by BATSE. HETE-2 made the first observations of long GRBs spatially associated with Type Ic supernovae. More recently, the Swift satellite is a currently operating mission with its Burst Alert Telescope (BAT) that detects and locates GRBs within 0.1°. In addition, it also carries an X-ray Telescope (XRT) and an Ultra-Violet and Optical Telescope (UVOT) which when slewed to the burst lo-

Table 1. List of past and operating space borne instruments that have detected GRBs along with the approximate numbers of GRBs detected by them as of August 2011.

Instrument	Observing energy range	Period of operation	GRBs detected
Vela 3-6	200 keV – 1 MeV	1967 – 1979	100
CGRO	50 – 300 keV (BATSE) 20 MeV – 30 GeV (EGRET)	1991 – 2000	2704 5
Konus/WIND	10 keV – 10 MeV	1994 – now	2114
BeppoSAX	2 – 600 keV	1996 – 2002	1082
HETE-2	2 – 400 keV	2000 – 2006	104
Integral	15 keV – 10 MeV	2002 – now	760
Swift	15 – 150 keV (BAT) 0.3 – 10 keV (XRT) 170 – 600 nm (UVOT)	2005 – now	612
AGILE	10 keV – 700 keV (SA+MCAL) 30 MeV – 30 GeV (GRID)	2007 – now	210 3
Fermi	10 keV – 40 MeV (GBM) 20 MeV – 300 GeV (LAT)	2008 – now	765 28

cation can successfully detect the GRB afterglows and locate the source with an accuracy of arcseconds. The success of the Swift mission has resulted in the measurement of the redshifts of nearly 200 GRB hosts out of a total of 600 GRBs detected. Swift made major breakthroughs in the understanding of the GRB afterglow emission that were hitherto unknown. Table 1 summarises the satellite observations and the on board γ-ray/X-ray detector characteristics as well as the total number of bursts detected by them as of September 2011 (updated version of the table in Bouvier 2010).

The precise location of GRBs is a challenge since GRBs are relatively short transient events which do not repeat and that they occur randomly in time and space. As a result, a majority of the early GRB missions before BATSE could not localise GRBs. BATSE was the first mission which could detect and locate a GRB within a couple of degrees. The angular resolution of BATSE was still too coarse to repoint optical or X-ray telescopes to the location of the explosion (which have a small field-of-view necessitating a few arc-minute location accuracy) to search for a burst counterpart the possible existence of which was theoretically predicted at the time (Rees & Mészáros 1992; Mészáros & Rees 1993). Early attempt to locate a GRB precisely was made by the Inter-Planetary Network (IPN[1]) which consists of a group of spacecrafts (so far 27 spacecrafts have participated in this network) equipped with γ-ray detectors. By timing the arrival of γ-rays from a burst at several spacecrafts the burst could be localised with an accuracy depending on the number of satellites detecting it. However very few bursts were located by this technique and

[1] `http://www.ssl.berkeley.edu/ipn3/`

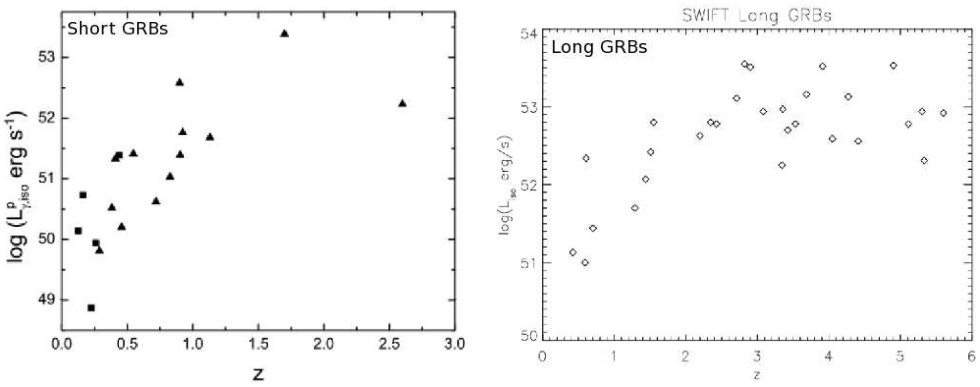

Figure 2. Two-dimensional luminosity-redshift distributions of short (Virgili et al. 2009) and long (Cabrera et al. 2007) GRBs using the recent Swift observations. The very high redshift GRB 090423 at $z \sim 8.2$ (Tanvir et al. 2009) or GRB 090429B at $z \sim 9.4$ (Cucchiara, Levan & Fox 2011) has not been included in this plot.

even when successful, the time delay was too long to be useful for follow-up observations at other wavelengths.

A breakthrough happened in early 1997, with the Dutch/Italian satellite BeppoSAX which was equipped with a wide angle GRB detector and X-ray telescopes with coded aperture. As soon as a GRB was detected by the on board wide-field camera (WFC) the satellite could slew such that the GRB source is in the field of view of the X-ray detectors which could then locate it, within hours, with in a few arcmin accuracy. This allowed the detection of the first fading X-ray emission from a long burst GRB 970228 leading to the improved localisation of the source accurate enough to facilitate follow-up observations at optical wavelengths for the first time. These observations initially identified a fading optical counterpart (van Paradijs et al. 1997), and, after the burst had faded, long duration deep imaging identified a distant host galaxy with a redshift $z = 0.498$ at the location of the burst. The redshifts are usually measured from the emission lines or the absorption features of the host galaxies imposed on the afterglow continuum. GRB 970508 was the first GRB for which the afterglow was concurrently observed over the whole electromagnetic spectrum a few hours after the burst. This was also the first GRB whose distance was estimated by measuring its spectroscopic redshift (Metzger et al. 1997). BeppoSAX thus paved the way for detections of more host galaxies and redshifts through spectroscopy of the GRB host galaxies, and settled the question of cosmological origin for long GRBs once and for all. The distance measurement of GRBs opened the door to the study of intrinsic properties of their sources for the first time. The typical γ-ray fluences measured by BATSE are of the order of 10^{-5} erg cm^{-2} which translates to an equivalent isotropically-emitted energy of $E_{\rm iso} \sim 10^{53}$ erg at the source. The total γ-ray fluence can be significantly smaller if the emission is beamed which is most likely the case.

Fig. 2 shows the isotropic energy distribution of GRBs as a function of redshift for short and

long GRBs. Considering the limited number of short GRBs with redshifts the two distributions do not seem to be very dissimilar (see §3.1 for details on burst classification).

In §2 the current theoretical understanding of GRB prompt and afterglow emissions are briefly explained. While §3 gives a brief description of the observational status prior to the launch of Fermi, §4 describes the Fermi instrumentation and its synergy with other γ-ray missions currently operating. §4.3 and 4.4 describe the latest observational results relating to both temporal and spectroscopic aspects of GRBs respectively. In §5 a brief description is given of the inferred results on GRBs as a class as well as some applications of Fermi GRB results relating to the attenuation of high energy γ-rays from distant sources and fundamental physics. Finally the paper concludes by identifying some of the important prospects of future breakthroughs in the understanding of GRB astrophysics when the new ground based multi-wavelength observatories become operational. In the next section we plan to present the basic understanding of what is generally believed to be responsible for the GRB phenomenon primarily for the benefit of beginners in the field.

2. Theoretical understanding of GRB physics

2.1 Progenitor and central engine

In the following sections we outline the observations that support these theoretical conclusions as well as those that often challenge them. Our understanding of the physics of GRBs is still far from definitive; however, there is a general agreement in the community that the progenitors of the long duration ($T_{90} > 2$ s) bursts are associated with the deaths of massive stars in a specific kind of supernova-like event commonly referred to as a collapsar or hypernova. A merger of two compact objects, such as two neutron stars or a neutron star and a stellar mass black hole is believed to be giving rise to short duration ($T_{90} \leq 2$ s) GRBs. For a more detailed discussion on burst durations see Section 3.1.

2.2 Fireball model

Several models have been proposed to explain the γ-ray emission mechanisms following the cataclysmic events mentioned above. Observational data outlined so far led over the years to the development of the well accepted GRB 'standard model' that describes the main properties of the GRBs with standard physics applied to somewhat 'exotic objects'. The widely accepted interpretation of the GRB phenomenology is that the observable effects are due to the dissipation of the kinetic energy of a relativistic expanding wind, a 'fireball', regardless of the nature of the underlying central engine (Cavallo & Rees 1978). No known process in the Universe can produce this much energy in such a short time. The GRB central engine, resulting from the collapse, produces collimated jet mainly composed of electrons, positrons, photons and a small amount of baryons moving at relativistic speeds. The outflow wind is believed to be highly inhomogeneous and the

high density regions can be assimilated to separate shells propagating at various velocities. The observed prompt emission in the γ-ray energy band would be mostly synchrotron radiation produced by the radially propagating electrons accelerated during collisionless shocks inside these jets.

2.3 Relativistic expansion and pair opacity

In this section we describe why the observation of GRB prompt emission can only be explained by highly relativistic outflows. Rapid rise times as short as 0.2 ms (Bhat et al. 1992) and durations as short as 1 ms (Fishman et al. 1994) imply that the observed emission regions are compact, $r_0 \sim 10^7$ cm. In addition, the high γ-ray luminosities observed by the detectors coupled to the cosmological distances of the source, $L_\gamma \sim 10^{52}$ erg s^{-1}, should result in a very high opacity of the GRB wind to γ-rays due to pair creation since the energy of observed γ-ray photons is above the threshold for pair-production. The density of photons at the source n_γ, is approximately given by

$$L_\gamma = 4\pi {r_0}^2 c n_\gamma \epsilon,$$

where $\epsilon \simeq 1$ MeV is the characteristic photon energy. Using $r_0 \sim 10^7$ cm, the optical depth for pair production at the source is

$$\tau_{\gamma\gamma} \sim r_0 n_\gamma \sigma_{\rm T} \sim \frac{\sigma_{\rm T} L_\gamma}{4\pi r_0 c \epsilon} \sim 10^{15}$$

where $\sigma_{\rm T}$ the Thompson cross-section. This is obviously in contradiction with the observation since a large amount of photons with energy above the threshold are actually detected by telescopes. This is the so-called 'compactness problem' in γ-ray burst astrophysics. The observation of γ-ray flux above ~ 1 MeV in several GRBs shows that pair creation is not predominant in the emission wind implying a low density of photons above the pair creation threshold at the source. This problem can be solved when we consider an expanding relativistic wind. Due to relativistic effect, photons below the pair creation threshold in the comoving frame are blue shifted and can appear to be above the pair-production threshold in the observer frame. Relativistic expansion thus provides a very efficient way of reducing the rate of pair creation in the moving source frame since the photons are softer by a factor of Γ, where Γ is the Lorentz factor of the relativistic flow. In addition the size of the emission region becomes $\Gamma^2 c\Delta t$ and the density of photons is thus reduced considerably (Δt is the observed variability time scale). Moreover, relativistic beaming implies that we observe only a small fraction $1/\Gamma$ of the source irrespective of the opening angle of the jet. Hence the angle at which the photons collide must be less than the inverse of the bulk Lorentz factor Γ^{-1} of the relativistic flow which drastically reduces the effective pair production cross-section if Γ is large. As a result, for a differential photon spectrum, $E^{-\alpha}$, the source becomes optically thin if $\Gamma \geq 100$ assuming $\alpha \sim 2$ (Piran 1999; Lithwick & Sari 2001). A general expression for the lower limit of the bulk Lorentz factor so that the source is transparent to a γ-ray photon of observed energy E_γ is (Waxman 2003).

$$\Gamma \geq 250 \left[\left(\frac{L_\gamma}{10^{52}\ {\rm erg\ s^{-1}}} \right) \left(\frac{E_\gamma}{100\ {\rm MeV}} \right) \left(\frac{\Delta t}{10^{-2}\ {\rm s}} \right) \right]^{\frac{1}{6}}$$

However, the most energetic GRB photons whose energies are above E_γ may still suffer from absorption leading to pair production in the GRB winds (Li et al. 2003). This may lead to energy dependent optical depth consequently giving rise to the delayed emission of higher energy γ-rays (Pe'er & Waxman 2005). Further discussion on this is in §4.4.1.

2.4 Fireball evolution

A fireball is essentially a dynamic object whose properties quickly evolve with time. It can be characterised by an initial energy E_0 and a radius $R_{\rm in}$, while the energy to mass ratio, $\eta = E_0/M_0c^2$ with $M_0 \ll E_0/c^2$, M_0 represents the baryon loading factor of the fireball and η the mean energy per baryon.

2.4.1 *Acceleration*

The initial optical depth being extremely high as mentioned before, the radial expansion of the fireball is a consequence of the highly super-Eddington luminosity where the internal energy is converted into kinetic energy. As the fireball cools during its expansion, its temperature varies as $T_\gamma \propto R^{-1}$. Since the total energy E_0 is constant, the bulk Lorentz factor increases linearly with R, $\Gamma \propto R$, until it saturates at a value $\Gamma_{\rm max} = \eta R_{\rm in}$. The radius of the fireball, where the bulk Lorentz factor reaches $\Gamma_{\rm max}$, is called the saturation radius, $R_{\rm s}$. Beyond the saturation radius, the bulk Lorentz factor Γ coasts at this value of $\Gamma_{\rm max}$. In this initial phase, the wind is optically thick and it is usually believed to become optically thin at the photospheric radius ($R_{\rm ph} \approx 10^{11} - 10^{12}$ cm). Before $R_{\rm ph}$, the photons and the electrons are in thermal equilibrium and the electron velocity distribution is Maxwellian. Beyond the saturation radius, the shells propagate in the jet at the constant velocities until the broadening radius ($R_{\rm is}$) where the shells expand indicating the beginning of the so-called internal shock phase (Rees & Mészáros 1994; Narayan, Paczynski & Piran 1992; Paczynski & Xu 1994).

2.4.2 *Internal shocks*

During the internal shock phase ($R_{\rm is} \approx 10^{14} - 10^{15}$ cm), faster shells catch up with slower ones leading to mildly relativistic collisionless diffusive shocks where the charged particles present in the shock region are accelerated. During the internal shock phase, charged particles with enough energy would be accelerated by scattering off the magnetic perturbations in the up stream or down stream shells. This acceleration mechanism is called the second order Fermi process. During this process the charged particles may cross the shock front multiple times where they are accelerated through first order Fermi processes. The first order Fermi process is much more efficient than the second order and the former process imparts the same amount of energy to the charged particle whether it crossed the front upstream or downstream. A charged particle performs a Fermi cycle

when crossing the shock front twice. It can take several Fermi cycles before gaining too much energy and escape.

If the photospheric radius $R_{\rm ph} < R_{\rm is}$, then the wind becomes optically thin before the internal shock phase starts, and a thermal emission can be observed first (Rees & Mészáros 1994). During the internal shock phase, the charged particles (mostly electrons) are accelerated through Fermi processes as discussed above. The electron energy distribution resulting from Fermi acceleration is a power law, and the final electron distribution would be a Maxwellian deformed above the Fermi energy threshold and with an extended power law tail. The γ-ray emission observed during the prompt phase of GRBs would be mostly the synchrotron emission from the electrons which propagate and are accelerated within an intense magnetic field. Each peak seen in the prompt emission light curves would correspond to an individual shock resulting from the collision of a pair of shells with unequal Lorentz factors. Protons could also be accelerated in these shocks, however, the acceleration time is much longer than that for electrons. Protons thus accelerated could produce synchrotron emission at higher energies. If $R_{\rm ph} > R_{\rm is}$, then the internal shock phase starts while the wind is still optically thick. This would result in heating the shells which in turn results in changing the electron distribution and the temperature of the photosphere while the jet becomes optically thin.

Thus, the variability of the light curve reflects the variable activity of the central engine. The total duration of the GRB corresponds to the total duration of the central engine activity. The main advantage of this model is that internal shocks are expected naturally in the baryonic outflow and they can easily explain the rapidly variable and diverse light curves of prompt γ-ray emission. In addition, the simplest interpretation of the emission as synchrotron radiation is roughly in agreement with the observed burst prompt emission spectra. The electrons have typical Lorentz factors in the range 10^2–10^3 and gyrate in a $\sim 10^6$ G magnetic field producing ~ 100 keV synchrotron emission (Nakar 2007). The main disadvantage of internal shock model is its efficiency. Internal shocks are expected to radiate only a small fraction ($\sim 1\%$) of total energy flow (Daigne & Mochkovitch 1998) whereas the observations suggest that the γ-ray efficiencies are much higher (Bloom et al. 2006).

During the internal shock phase, the width of the shells expands as the radius increases reducing the density of the magnetic perturbations they contain. Then, shocks occurring far from the central engine are less efficient leading to particles with lower energy. In addition, the magnetic field strength decreases with the distance to the central engine, reducing the intensity and the maximum energy of the synchrotron emission.

2.4.3 *External shock*

The internal shock phase ends at the decelerating radius $R_{\rm es}$ (10^{16}–10^{17} cm), when the wind is slowed down by interacting with the interstellar medium in a relativistic shock, called external shock. The external shock would be composed of two shocks, the forward shock which expands in the direction of the interstellar medium, and the reverse shock which comes back in direction

of the central engine. The position of $R_{\rm es}$ depends on the density of the interstellar medium. In the case of the compact object merger, GRBs are believed to happen in low interstellar density environment (compact objects can migrate far from the star forming region before merging), while in the hypernova scenario GRBs occur mostly in the star forming region where the interstellar density is high. The surroundings of a hypernova are enriched by the stellar wind of the star before the collapse. $R_{\rm es}$ is therefore believed to be larger for the merger scenario than that for the hypernova. During the external shock, charged particles of the interstellar medium and of the wind would be accelerated, and would radiate through synchrotron and/or inverse-Compton scattering process, which would be responsible for the afterglow emission observed from radio wavelengths to X-rays and maybe γ-rays (see §2.6 for more details).

External shocks could also produce the observed prompt emission according to some models. In these models radiation pulses are emitted when a relativistic shell ejected by the GRB central engine is decelerated by the circum-burst material (Mészáros & Rees 1993). A homogeneous medium leads to a single pulse but an irregular, clumpy environment can produce a complex profile if a large number of small clouds are present (Dermer & Mitman 1999). One major difficulty with this model is to explain the rapid variability observed in GRB light curves at various energies. In this case the clumpiness has to be of the order of $\sim \Gamma_{\rm f} c\Delta t/(1+z)$ where Δt is the variability time scale observed in the GRB light curve and $\Gamma_{\rm f}$ is the Lorentz factor of the forward shock. However this process has been shown to be very inefficient (Sari & Piran 1997). Variability can be recovered while maintaining high efficiency if the shell that moves with a bulk Lorentz factor $\Gamma_{\rm f}$ contains emitting clumps.

The external shock model has been successfully used for explaining the GRB afterglow emission observed from hours to days from radio wavelengths to X-rays and γ-rays following the prompt emission, and even for years at radio wavelengths. The GRB afterglow emission is presented in detail in §2.6.

Fig. 3 shows a sketch of the γ-ray burst production mechanism, the prompt emission regions during the internal shocks as well as the afterglow emission from the external shocks.

2.5 Prompt emission from a magnetised flow

There are several alternative models for the prompt GRB emission, which so far have not found wide use for explaining the observations. The most plausible of these, despite the technical difficulties which impair its applicability, considers the main γ-ray burst emission to arise from magnetic reconnection or dissipation processes, if the ejecta is highly magnetised or Poynting flux dominated. If the outflow energy is carried mostly by Poynting flux until where the interaction with the external medium starts, the dissipation of the bulk energy into internal energy cannot occur through internal shocks. In this case the energy source of the radiation is most likely magnetic dissipation. Lytikov & Blandford (2003) suggest that electromagnetic current-driven instabilities dissipate magnetic energy into heat and high energy particles. The propagation of

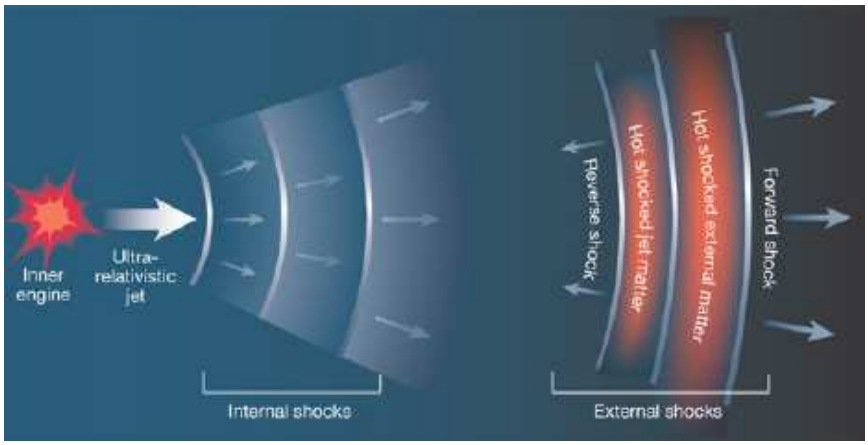

Figure 3. Sketch showing the different phases involved in the 'fireball' model with internal shocks producing the γ-ray prompt emission and external shock with the interstellar medium or the star wind responsible for the afterglow phase observed in radio, optical, X-rays, γ-rays (Piran 2003).

these high energy particles within a strong magnetic field, is the source of the observed prompt γ-ray emission.

Thompson (2006) suggests a model which is a flow consisting of a combination of a strong magnetic field and pair-radiation plasma. In this model the radius in which the outflow becomes optically thin is determined by the pair enrichment of the ambient medium through the interaction with the flow radiation. The prompt emission is generated by the inverse Compton scattering of the seed photons that are carried in the flow by pairs which are accelerated by the reconnecting magnetic field. The energy at the peak of the prompt emission spectrum reflects the temperature of these seed photons Lorentz boosted to the observer frame.

2.6 GRB afterglow emission

The prompt emission is usually followed by a longer-lived 'afterglow' emitted at longer wavelengths. Afterglows are now known to be broad-band, having been detected in the X-ray, the optical/infrared and the radio bands. X-ray afterglows are mostly decaying when they are detected. Optical afterglows are generally decaying, with an initial early rising lightcurve having been caught in only a few bursts (e.g. GRB 970508, GRB 990123). In each band, the general power-law decay behaviour can be summarised as: $t^{\alpha}\nu^{\beta}$ where $\alpha \sim -0.9(-1.0)$ and $\beta \sim -1.4(0.7)$ for X-ray (Piro et al. 2001) (optical, Zeh, Klose & Kann 2006) afterglows. GRB 970228 was the first GRB for which an X-ray afterglow was observed (Costa et al. 1997). The X-ray emission was fading fast following a power law $F(t) \sim T^{-1.3\pm0.1}$. This also led to the detection of the first optical afterglow from this GRB (van Paradijs et al. 1997). Very often there are var-

ious types of deviations from the simple power law decay. These include steepenings, bumps and wiggles (e.g. GRB 021004; GRB 030329); Essentially every GRB with an afterglow detection has an underlying host galaxy. The GRB host galaxy properties (e.g. magnitude, redshift distribution, morphologies) are typical of normal, faint, star forming galaxies (Djorgovski et al. 2003). The GRB afterglow's positional offsets with respect to the host galaxy are consistent with GRBs being associated with the star forming regions in the galaxies (Bloom et al. 1998). In the radio band, on the other hand, the spectral index is generally positive for the observations which are typically in the 5 and 8.5 GHz bands. The light curves usually do not follow a simple power law decline (Frail et al. 2003). Some sources can be observed on timescales of years, and a late-time flattening (with respect to the standard fireball model) is often observed (Frail et al. 2004).

2.6.1 *Standard afterglow model*

The standard afterglow model assumes a highly relativistic expansion of a spherical outflow in the adiabatic regime into a homogeneous external medium. The external shocks appear when the relativistic outflow is slowed down in the interstellar medium (ISM) surrounding the source or the stratified wind ejected by the progenitor star prior to the collapse (Rees & Mészáros 1992). Generally two shocks form: an outgoing shock, called the forward shock, that propagates into the surrounding medium and a reverse shock that propagates back into the ejecta. The external shock successfully explains multi-wavelength afterglow radiation which begins at a distance where most of the energy of the ejecta is transferred to the medium. However the assumptions in the standard model are too simplistic while the real life situations more complex. The impact of the reverse shock is invoked to explain the early optical flashes while the beaming of the outflow within a jet of solid angle $\Omega_{\rm j}$ is an ingredient to reduce the energetics of GRBs as mentioned before.

In order to produce the observed spectrum during both the afterglow and the prompt emission phases, electrons must be accelerated in the collisionless shocks to a power law distribution, $dn_{\rm e}/d\Gamma_{\rm e} \propto \Gamma_{\rm e}^{-p}$ with $p \simeq 2$ where $\Gamma_{\rm e}$ is the electron Lorentz factor. Such a distribution is expected in the internal shocks, which are mildly relativistic. Numeric and analytic calculations of particle acceleration via the first order Fermi mechanism in relativistic shocks show that similar indices, $p \approx 2.2$, are obtained for highly relativistic shocks as well (Bednarz & Ostrowski 1998; Kirk et al. 2000). The spectrum of radiation is likely to be due to synchrotron radiation, whose peak frequency in the observer frame is $\nu_m \propto \Gamma_{\rm max} B' \Gamma_{\rm e}^2$, where the comoving magnetic field B' and electron Lorentz factor $\Gamma_{\rm e}$ are likely to be proportional to $\Gamma_{\rm max}$ (maximum value of the bulk Lorentz factor). This implies that as $\Gamma_{\rm max}$ decreases, so will ν_m, and the radiation will move to longer wavelengths. Consequently, the burst would leave a radio remnant weeks after the explosion (Paczynski & Rhoads 1993). The observation of linear polarisation at the few percent level observed in a number of optical or IR afterglows (van Paradijs, Kouveliotou & Wijers 2000) supports the paradigm of synchrotron emission as the dominant emission mechanism in the afterglow.

2.6.2 *Prompt flashes and reverse shocks*

The first optical brightening following a γ-ray burst was observed from GRB 970508. More recently the observation of extremely bright ($m_v \sim 9$) optical flash in the burst GRB 990123 which is interpreted as due to reverse shock (Sari & Piran 1999) even though a prompt optical flash could be expected from either internal shock or reverse shock of external shock. The decay rate of the optical flux from the reverse shock is much faster (and that from internal shock is even faster) than that of the forward shock. Generally reverse shock is expected to be mildly relativistic and hence radiate much softer radiation than the forward shock (Mészáros 2006). After the launch of Swift, new prompt optical observations with robotic telescopes have greatly added to the phenomenology of prompt flashes which are consistent with the reverse shock interpretation.

Currently, Swift is the only mission designed to detect GRB afterglows. The BAT, with its large field of view of 2 steradians, can detect and locate a GRB, as well as compute burst positions on board with arc-minute positional accuracy. The spacecraft then slews to this position and the XRT takes images to obtain spectra of GRB afterglows. The images are used for higher accuracy position localisations, while light curves are used to study flaring and long-term decay of the X-ray afterglow. At the same time the UVOT also takes images and obtains spectra (via a grism filter) of GRB afterglows. The images are used for 0.5 arcsecond position localisations and following the temporal evolution of the UV/optical afterglow. Spectra are taken for the brightest UV/optical afterglows, which can then be used to determine the redshift via the observed wavelength of the Lyman-alpha cut-off. Accurate localisations are transmitted in real time to enable ground based observatories to carry out multi-wavelength follow-up observations of the GRB afterglows.

Fig. 4 is a sketch of a typical afterglow observed by Swift (Zhang et al. 2006). It consists of a fast decay phase (I) followed by a plateau region (II), which is a major Swift discovery, lasts for a few thousand seconds and then reaches typical afterglow decay with a slope of ~ -1.2 (III) as already observed before Swift.

2.7 Measurement of the jet opening angle

The spherical assumption is valid even when considering a relativistic outflow collimated within some jet of solid angle $\Omega_j < 4\pi$, provided the observer line of sight is inside this angle, and $\Gamma_e \gtrsim \Omega^{-1/2}$ (Mészáros, Laguna & Rees 1993) so the light-cone is inside the jet boundary and the observer is unaware of what is outside the jet. However, as the ejecta is decelerated, the Lorentz factor eventually drops below this value, and a change is expected in the light curves (Rhoads 1999). It is thought that this is what gives rise to the achromatic breaks seen in the light curves of many optical afterglows (Frail et al. 2001)

The jet opening angle can be obtained from the observer time t_j at which the flux F_ν decay rate achromatically changes to a steeper value, assuming that this corresponds to a causal angle

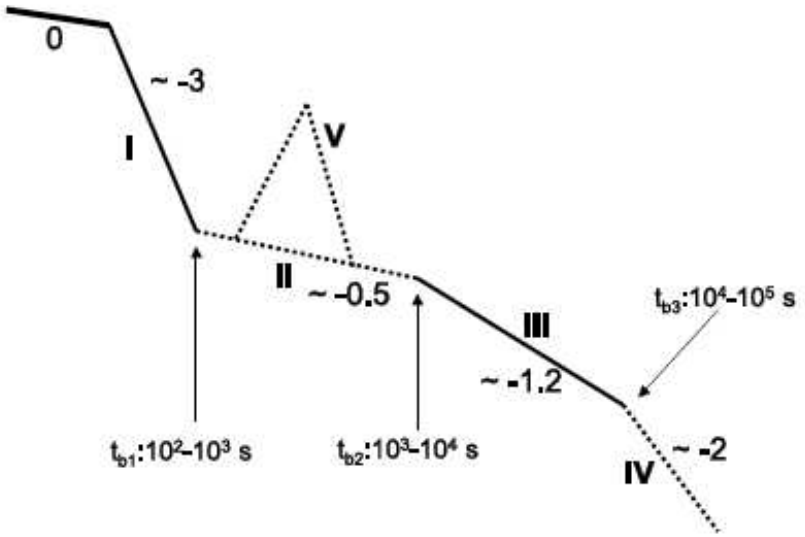

Figure 4. Sketch of an afterglow light curve based on Swift's observations. Phase '0', corresponds to the end of the prompt emission. Four power-law light-curve segments together with a flaring component are identified in the afterglow phase. The components marked with solid lines are the features common to most long GRBs, while the ones marked with dashed lines are observed in only a fraction of GRBs. The phase II is often called the plateau. The typical spectral indices of the power law decay are shown for each segment. The break between regions III and IV occurs simultaneously for several observed frequencies (achromatic break) and is related to the geometry of the GRB relativistic jets. For some bursts the break is not achromatic.

$\Gamma_e(t)^{-1}$ having become comparable to the jet half-angle and larger later on. However the detailed simulation studies show that for off-axis observers, the observable jet break can be delayed up to several weeks, potentially leading to overestimation of the beaming-corrected total energy (van Eerten, Zhang & MacFadyen 2010). In addition, achromatic jet breaks are relatively rare in the literature. Different explanations for the lack of truly achromatic breaks have been put forth. It was shown recently that in general γ-ray burst afterglow jet breaks are chromatic across the self-absorption break (van Eerten et al. 2011).

2.8 GRB as UHECR sources

One of the outstanding problems in astronomy is the origin of ultra-high energy cosmic rays (UHECR). The local ($z = 0$) energy production rate in γ-rays by GRBs is roughly given by the product of the characteristic GRB γ-ray energy, $E \approx 10^{53}$ erg and the local GRB rate. Under the assumption that the GRB rate evolution is similar to the star formation rate evolution, the local GRB rate is ~ 0.5 Gpc^{-3}yr^{-1}, implying a local γ-ray energy generation rate $\approx 10^{44}$ erg Mpc^{-3} yr^{-1}. The energy observed in γ-rays reflects the fireball energy in accelerated elec-

trons. Thus, if accelerated electrons and protons carry similar energy (as indicated by afterglow observations) then the GRB production rate of high energy protons is remarkably similar to that required to account for the flux of $> 10^{19}$ eV cosmic rays (Waxman 2003). Based on these arguments GRBs have been proposed as a likely source of UHECRs (Waxman 1995; Dermer 2002). However there are some questions unanswered. These include the limitations to the highest energy attainable by protons around the bursts' shocks, the spectral slope at the highest energies, the total energy released in non-thermal particles, and the occurrence of doublets and a triplet in the data reported by the Akeno Giant Air Shower Array (AGASA). Considering the uncertainties and the apparent agreement in the energy budget GRBs seem to be a strong candidate for the source of UHECRs. In addition, the computed resulting particle spectrum at Earth, fits the High Resolution Fly's Eye (HiRes) and AGASA data to within statistical uncertainties (Vietri, De Marco & Guetta 2003).

3. Observational status: pre-Fermi era

3.1 Prompt emission durations and two GRB classes

GRB time profile is unique and unpredictable. Some are smooth and exhibit a fast rise and exponential decay (often referred to as 'FRED') type profile while others are highly variable with several overlapping narrow pulses (see Fig. 5). GRBs exhibiting FRED type light curves are shown to be not any different from other type of GRBs (Bhat et al. 1994). One clear example of uniqueness was demonstrated by the lack of success in a search for gravitational lensing in GRBs (Davidson, Bhat & Li 2011) where searches are carried out for similar temporal and spectral characteristics among several hundreds of GBM GRB light curves. As a result, morphological GRB classification attempts have not been successful and the only established division of bursts into classes with different temporal characteristics is based on their $T_{90}(T_{50})$ durations defined as the times during which 90% (50%) of the total signal counts (or fluence) are collected (Kouveliotou et al. 1993). The burst durations when measured in the 50–300 keV energy range, have been found to distribute bimodally, with over 75% of the events belonging in the long class (> 2 s).

McBreen et al. (1994) and later Horváth (2002) showed that T_{90} of both long and short GRBs follow log-normal distributions separately (see Fig. 6). The distributions peak at ≈ 0.8 s for short bursts and at ≈ 32 s for long bursts. In general, short bursts are often found to be less luminous by about 3 orders of magnitude leading to the possibility that excess of long GRBs compared to short ones is most likely an instrumental selection effect (Nakar 2007).

Hardness ratios of short GRBs compared to those of long ones show that the former are on the average harder. Kouveliotou et al. (1993) combined this result together with the bimodal duration distribution to suggest that short and long GRBs are two distinct populations. Fig. 7 shows a plot of the average $E_{\rm peak}$ of a set of BATSE GRBs in different duration ranges as a function T_{90} clearly showing that on the average the mean $E_{\rm peak}$ of short GRBs is almost twice as large as that for long GRBs supporting the dual population hypothesis (Paciesas et al. 2001).

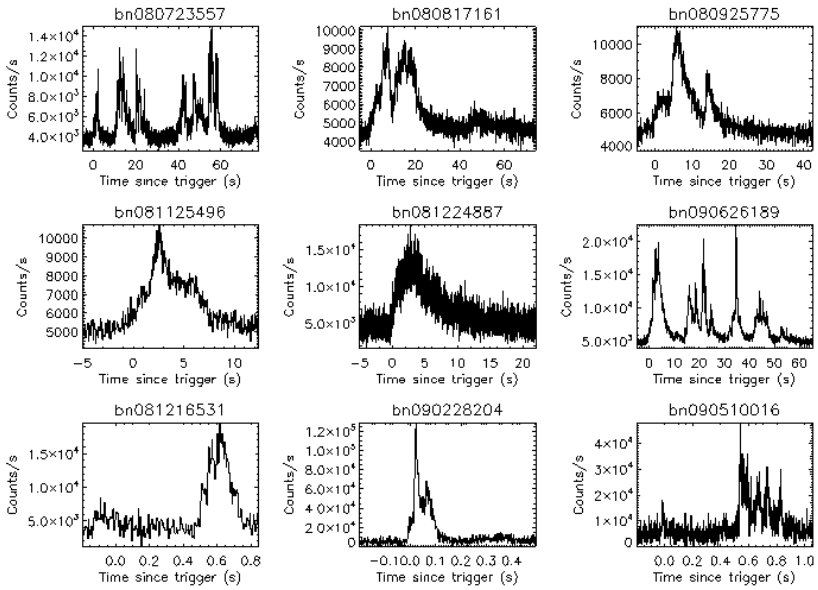

Figure 5. A sample GRB light curves from the GBM experiment demonstrating their diversity and uniqueness. The first two rows of light curves are from long GRBs ($T_{90} > 2$ s) while the last row shows light curves from short GRBs ($T_{90} \leq 2$ s).

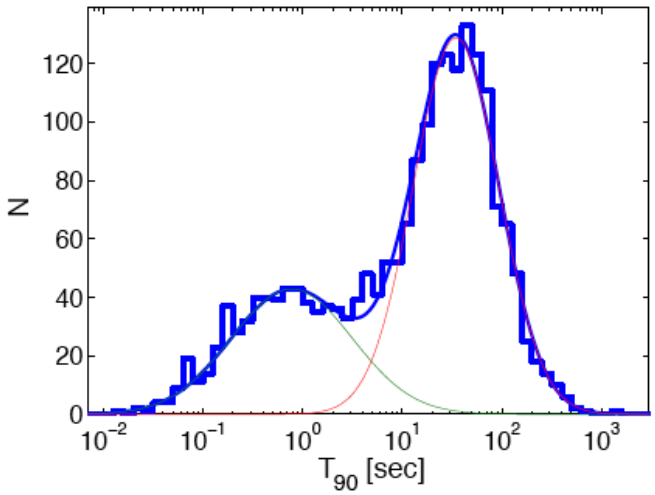

Figure 6. The bimodal duration distribution of GRBs. The blue histogram represents the distribution of durations for 2041 bursts detected by BATSE. The histogram is well fit by two log-normal functions (blue and red thin solid lines) and their sum is shown in thick blue line (Horváth 2002).

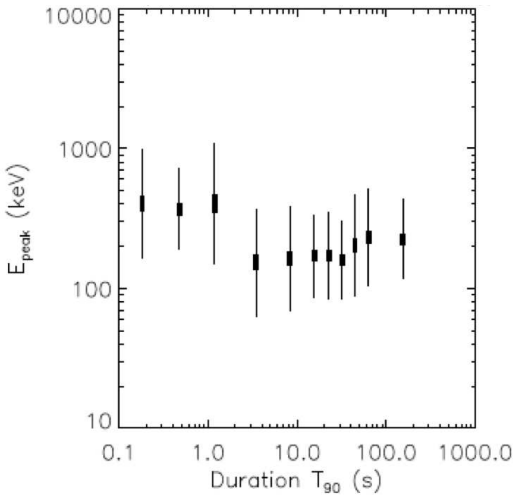

Figure 7. One of the spectral parameters ($E_{\rm peak}$, see §3 for details) as a function of burst duration (T90) for spectral fits of a Comptonised model to BATSE GRBs. The vertical bars show the width of a Gaussian fit to the parameter distribution within a duration bin. Thick vertical bars show the error on the mean of each. The average value of $E_{\rm peak}$ for short bursts is almost a factor of 2 larger to that of long GRBs.

3.2 Spectroscopy of the prompt emission

Gamma-ray spectroscopy with detectors such as BATSE or later GBM, is not straightforward like that with optical or X-ray telescopes. These γ-ray instruments with high background are actually not measuring photon numbers directly but counts. The detector response matrices, which allow the conversion from photon space to count space are usually not invertible. It is then not possible to measure a photon flux from the measured count flux. The only way to determine the best fit to a gamma-ray spectrum is to assume a spectral model and to optimise its parameters by fitting the model to the data following this procedure:

- a spectral photon model is assumed;
- this photon model, with chosen initial parameters, is folded through the instrument response function to convert photon numbers to counts to be able to compare the resulting model count spectrum with the real count spectrum measured by the instrument;
- the previous step is repeated by varying the model parameters until the fit convergence criteria is reached.

This methodology is a major inconvenience to measuring the real photon spectrum since the observed spectrum could only be compared with the deconvolved model dependent spectrum. This makes the identification of the spectral shape more difficult.

Unlike their light curves, the time-integrated spectra of GRBs do not show the same extent of diversity. Majority of the BATSE GRB prompt emission spectra in the keV–MeV energy range were adequately fit with an empirical function called the Band function (Band et al. 1993). The Band function, shown below, consists of two power laws, connected together at the break energy given by $E_{\rm peak}/(\alpha-\beta)$, with α and β the lower and the higher energy spectral indices respectively:

$$N(E) = A \begin{cases} \left(\dfrac{E}{100\ \text{keV}}\right)^{\alpha} \exp\left(-\dfrac{E(\alpha-\beta)}{E_{\rm peak}}\right) & \text{if } E < E_{\rm peak}, \\ \left(\dfrac{E_{\rm peak}}{100\ \text{keV}}\right)^{\alpha-\beta} \exp(\beta-\alpha)\left(\dfrac{E}{100\ \text{keV}}\right)^{\beta} & \text{if } E \geq E_{\rm peak}, \end{cases}$$

where $N(E)$ is the differential photon spectrum, E the photon energy in keV and A is the normalisation constant in photons $\text{s}^{-1}\text{cm}^{-2}\text{keV}^{-1}$ and $E_{\rm peak}$ corresponds to the maximum of the νF_{ν} (i.e. $E^2 N_{\rm e}$) spectrum when $\alpha > -2$ and $\beta < -2$ (Gehrels 1997).

Although purely empirical, the Band function is usually associated with the synchrotron emission from electrons that are propagating and accelerated within the GRB jet (Preece et al. 1998). However, the values of the Band low energy power law indices α are inconsistent with the synchrotron slow and fast cooling scenarios in 20% of the cases (Preece et al. 1998; Crider et al. 1997). For BATSE GRBs, the $E_{\rm peak}$ distribution peaks around 200 to 300 keV while the α and β distributions peak around -1 and -2 respectively (Goldstein et al. 2010). As mentioned before, the short GRBs are usually harder than the long ones with respect to both α and $E_{\rm peak}$ (Paciesas et al. 2003). A global hard to soft spectral evolution was reported by Ford et al. (1995) by fitting the time-resolved spectra to Band functions.

Briggs et al. (1999) showed that the time-integrated prompt emission spectrum of the bright GRB 990123 which was simultaneously observed with BATSE as well as the three other γ-ray detectors on board CGRO viz. the Oriented Scintillation Spectrometer Experiment (OSSE; Johnson et al. 1993), the Compton Telescope (COMPTEL; Ryan 1989) and the Energetic Gamma-ray Experiment Telescope (EGRET; Nolan et al. 1992), could be well fit with a single Band function across a large energy range from a few tens of keV to about 100 MeV (see Fig. 8). González et al. (2003) on the other hand reported a deviation from the Band function at high energies for one GRB 941017, that was detected with both BATSE and EGRET. The γ-ray emission excess over the Band function was adequately fit with an additional high energy power law. A time resolved spectral analysis showed that the additional power law component stayed constant across the burst while the Band function evolved as expected, with a global decrease of the emission intensity together with a softening of the spectrum. This high energy power law component was found to be inconsistent with the synchrotron shock model.

Delayed high energy γ-ray emission with respect to the main part of the prompt emission was reported in several cases (Sommer et al. 1994; Hurley et al. 1994). A classic example was the case of GRB 940217 when, among others, an 18 GeV photon was detected by EGRET, 90 min after the BATSE trigger time.

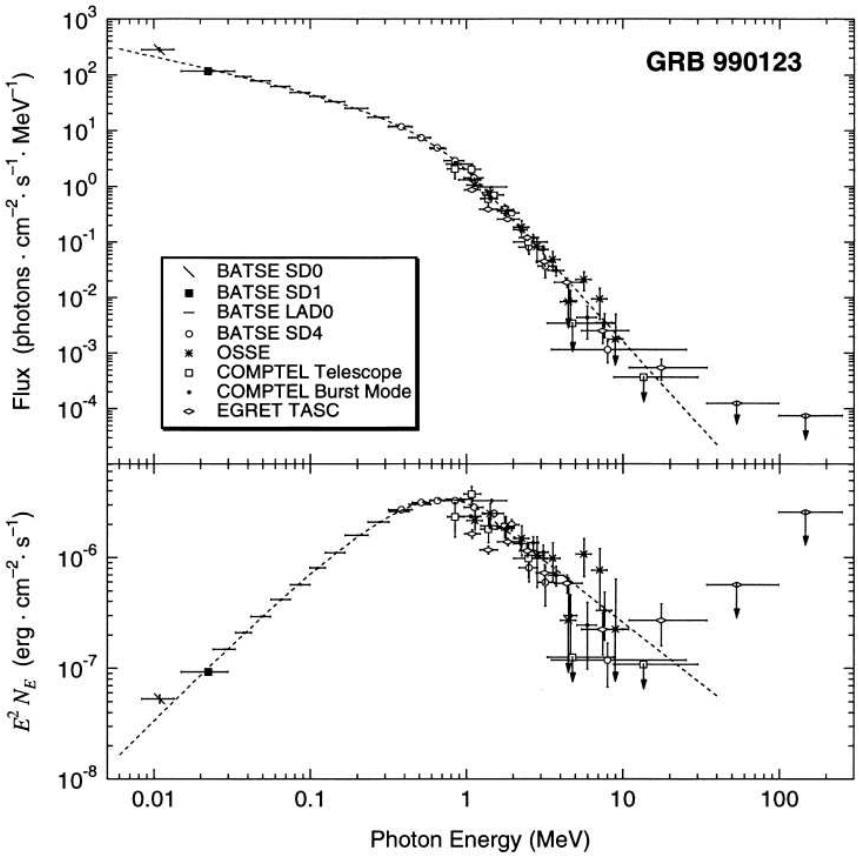

Figure 8. GRB prompt emission spectra in the BATSE Era were usually considered to be adequately fit with the empirical Band function even on large energy range in the γ-ray regime. Here is the case of the famous GRB 990123 that was simultaneously observed with the 4 instruments on-board CGRO (i.e. BATSE, OSSE, Comptel and EGRET) up to several tens of MeV. The top panel shows the spectrum of this GRB in photon flux units, while the bottom one corresponds to the νF_ν (i.e. $E^2 N_e$) spectrum. This bright GRB has a high E_{peak} around 1 MeV compared to average GRBs observed with CGRO (Kulkarni et al. 1999).

In general BATSE bursts exhibited non-thermal spectra in their prompt emission. However, the fireball model predicts and requires a photospheric emission simultaneously with the prompt emission (Rees & Mészáros 2005; Mészáros & Rees 2000). The existence of such a thermal emission component was claimed at least in some of the BATSE bursts (Ghirlanda, Celotti & Ghisellini 2003; Ryde 2004, 2005a; Ryde et al. 2010). While Ghirlanda, Celotti & Ghisellini (2003) tried to fit only a Planck function to the data, others were using a combination of a black body component and a power law (Ryde 2004, 2005a).

4. Observational status: Fermi era

4.1 Fermi Gamma-ray Space Telescope

The Fermi Gamma-ray Space Telescope (or Fermi for short) – formerly Gamma-ray Large Area Space Telescope (GLAST) – is a space based γ-ray observatory launched on 2008 June 11 to explore the gamma-ray sky. Fermi consists of two instruments on board viz. the Large Area Telescope (LAT) and the Gamma-ray Burst Monitor (GBM).

The LAT is an imaging high-energy γ-ray telescope covering the energy range from $\sim$ 20 MeV to more than 300 GeV[2]. The LAT is a pair-conversion telescope with a precision tracker and a hodoscopic calorimeter consisting of 16 modules in the form of a 4×4 matrix and a segmented anti-coincidence detector that covers the tracker array. Each tracker module has a vertical stack of 18 x, y tracking planes, consisting two layers (x and y) of single-sided silicon strip detectors. The 16 planes at the top of the tracker are inter-leaved with high-Z converter material (Tungsten). Every calorimeter module has 96 CsI(Tl) crystals, arranged in an 8 layer hodoscopic configuration with a total depth of 8.6 radiation lengths. The aspect ratio of the tracker (height/width) is 0.4 allowing a large field-of-view (2.4 sr). LAT has a programmable GRB trigger and data acquisition system. The vital specifications of LAT in comparison to those of EGRET are summarised in Table 2 (Atwood et al. 2009).

The GBM comprises 12 uncollimated Sodium Iodide (NaI(Tl)) detectors operating over the 8 keV to 1 MeV range, and 2 Bismuth Germanate ($Bi_4Ge_3O_{12}$ or BGO for short) detectors operating over the 150 keV to 40 MeV range. The axes of the NaI detectors are oriented such that they have the uniform view of the entire unocculted sky and the positions of GRBs can be derived from the measured relative counting rates, a technique previously employed by BATSE. Although GBM is smaller and slightly less sensitive than its predecessor BATSE, its extended energy range, from 8 keV to 40 MeV, combined with an improved data format, makes it an unprecedented all-sky instrument for time-integrated and fine-time resolved spectroscopy of transient sources like GRBs, Terrestrial Gamma-ray Flashes (TGFs), Soft Gamma Repeaters (SGRs), Solar Flares etc. The GBM flight software triggers on a GRB (or any fast transient) with a peak flux above 0.75 photons $cm^{-2}s^{-1}$ and locates it in the sky within an error of $\sim 15^\circ$ and transmits the information through Gamma-ray Coordinates Network (GCN[3]) within the first 8 seconds of a trigger to initiate follow-up observations with other instruments. Updates on location with an accuracy of $\sim 5^\circ$ are sent within next couple of seconds. More details on GBM detectors and data types may be found in Meegan et al. (2009). GBM also provides near real-time on-board burst-localisation to the Fermi spacecraft to repoint the LAT in direction of the source in order to increase its sensitivity to the burst and to detect possible high energy delayed emission from the source.

[2]So far spectroscopy only above 100 MeV is possible while new techniques are in the process of validation to decrease this threshold at least for spectroscopy of transient sources.

[3]`http://gcn.gsfc.nasa.gov/`

Table 2. LAT Specifications and Performance Compared with EGRET.

Quantity	LAT (Minimum Spec.)	EGRET
Energy Range	20 MeV – 300 GeV	20 MeV – 30 GeV
Peak Effective Area[a]	> 8000 cm^2	1500 cm^2
Field of View	> 2 sr	0.5 sr
Angular Resolution[b]	$< 3.5^\circ$ (100 MeV)	5.8° (100 MeV)
	$< 0.15^\circ$ (> 10 GeV)	
Energy Resolution[c]	$< 10\%$	10%
Dead-time per Event	< 100 μs	100 ms
Source Location Determination[d]	$< 0.5'$	$15'$
Point Source Sensitivity[e]	$< 6 \times 10^{-9}$ cm^{-2}s^{-1}	$\sim 10^{-7}$ cm^{-2}s^{-1}

Notes: (a) after background rejection; (b) single photon, 68% containment, on-axis (c) 1-σ, on-axis; (d) 1-σ radius, flux 10^{-7} cm^{-2}s^{-1} (> 100 MeV); (e) > 100 MeV, at high $|b|$, for exposure of one-year all sky survey, photon spectral index -2.

4.2 Synergy between Fermi and the other instruments

Currently, GBM is the best instrument to study GRB prompt emission in the keV–MeV energy range where the prompt emission is the most intense. With the LAT, our knowledge of the prompt emission at high energy is extended up to several tens of GeV. Even though Fermi is an outstanding observatory for studying the prompt emission, the poor location capabilities of GBM (several degrees) is a handicap for follow-up observations. To perform spectral analysis with GBM, detector response matrices must be generated based on the source location. Using an inaccurate localisation can lead to wrong responses if, for instance, a part of the spacecraft, such as a radiator, blocks one or more GBM detectors from the source. Accurate localisation is also necessary to repoint the ground based optical and VHE γ-ray telescopes (see §6.1 for details) that have narrow field of view. Without an accurate localisation of the source, we cannot get counter part signature at other wavelengths, nor host galaxy detection, nor redshifts. These observations are crucial to understand GRBs. Hence a good synergy of Fermi with other instruments is required. Obviously, the LAT can locate a GRB accurately enough to perform follow up observations with other instruments, but only a few GRBs (about 18) have been detected by the LAT (during first 2 years of operation) over a total ~ 500 GBM bursts, and the locations were obtained from ground analysis several hours after the burst trigger, which is late to initiate a successful follow-up observations.

IPN and Swift can provide good localisations. The IPN location is too delayed to be useful for follow-up observations as mentioned before. Swift detected $\sim 14\%$ of GBM GRBs during the first 2 years of operation, of which $\sim 12\%$ triggered the Swift BAT and the rest were discovered after ground analysis of BAT data. $\sim 1\%$ were located by the Swift XRT based on trigger from another instrument (Paciesas et al. 2011).

Detection of GBM GRBs with other gamma-ray instruments is also important to inter-calibrate the detectors. Table 3 lists the fraction of GBM GRBs detected simultaneously with other γ-ray instruments during the first 2 years operation.

Table 3. Fraction of GBM GRBs also detected with other gamma-ray instruments during the first 2 years till July 15, 2010.

Instrument	# of Observed GRBs simultaneously with GBM	Fraction of GBM GRBs (%)
Konus (WIND)	146	~ 30
Integral (Burst Alert System)	6	~ 1
Integral (SPI-ACS)	213	~ 43
Swift	68	~ 14
Super AGILE	5	~ 1
Fermi (LAT)	18	~ 4
RHESSI	33	~ 7
MAXI	4	~ 1
Suzaku (WAM)	200	~ 41

4.3 GRB temporal results

4.3.1 *Energy dependence of burst durations*

The observer frame GRB durations (as described in §3.1) measured are expected to suffer from relativistic effects. It was realised that the burst intensity could add unknown systematic errors in the estimation of durations as well (Bonnell et al. 1997). Often weaker GRBs have large errors on their estimated durations. See the recently published GBM 2-year burst catalog for a comprehensive summary of GBM GRB durations and fluences (Paciesas et al. 2011). Gruber et al. (2011) studied the GRB rest frame distributions of 32 GBM GRBs with known redshifts. They find that the T_{90} distribution in the GRB rest frame peaks at $\approx 10\,$s. Another important parameter that affects the estimation of T_{90} is the energy range (Richardson et al. 1996; Bissaldi et al. 2011). It has been found that on the average the burst durations fall with increasing energy as a power law with an exponent of ~ 0.4. However for a given burst the duration could evolve differently with energy. The T_{90} and T_{50} values for the GBM detected burst GRB 080916C are estimated in different energy bands using the GRB light curves summed over 4 bright NaI and 2 BGO detectors separately. The $T_{90}(T_{50})$ are plotted as a function of average energy and shown in Fig. 9. The BGO points are shown in purple. The slopes of the power law fits to the durations are also indicated in green. The values of the slopes (shown on the top right) are much shallower than -0.4.

4.3.2 *GRB spectral lags*

Temporal delays in the arrival of low-energy photons relative to that of high-energy photons, called spectral lags, are well known in GRBs. A general convention is positive spectral lag corresponds to an earlier arrival time of the higher energy photons. Spectral lags are traditionally measured between a pair of light curves of a GRB in 2 energy bands (25–50 and 100–300 keV

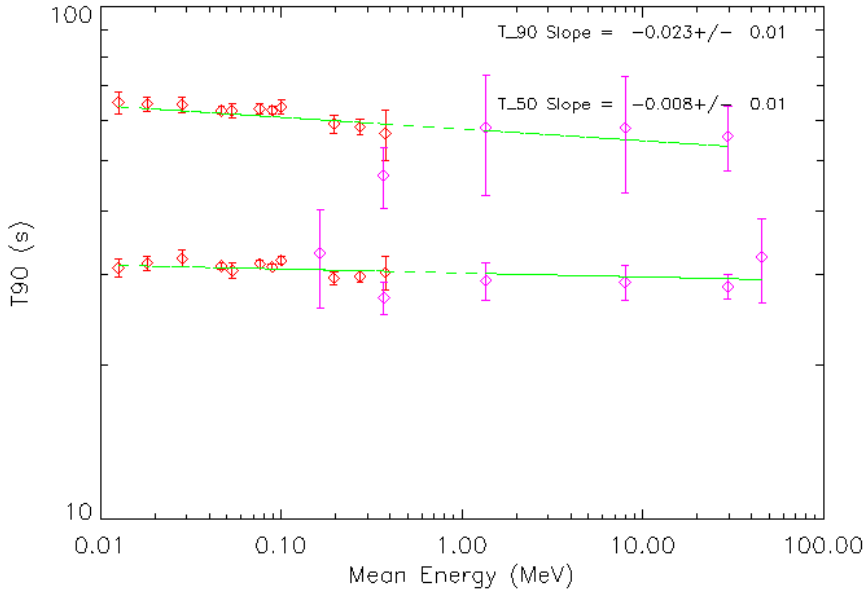

Figure 9. The upper plot shows the variation of T_{90} as a function of mean energy of the γ-rays. The straight line shows a power law fit to the data and the slope is indicated. Similarly the lower plot corresponds to T_{50} values of the same burst. The T_{90} and T_{50} values evolve differently and not consistent with the average behaviour.

for BATSE bursts). The standard method adapted is to compute the cross-correlation function (CCF) between the two light curves. The time lag at which the CCF peaks is defined as spectral lag. Generally the spectral lags of long GRBs are positive, a small fraction of them have been shown to exhibit zero or negative lags (Gupta, Das Gupta & Bhat 2002; Chen et al. 2005). One of the proposed explanations for the observed spectral lag is the spectral evolution during the prompt phase of the GRB (Dermer 1998; Kocevski & Liang 2003; Ryde 2005b). Due to cooling effects, $E_{\rm peak}$ moves to a lower energy channel after some characteristic time. When the $E_{\rm peak}$ moves from a higher energy band to a lower energy band, the temporal peak of the light curve also moves from a higher energy band to a lower one, which results in the observed spectral lag. In a recent study Peng et al. (2011) suggest that spectral evolution can be invoked to explain both positive and negative spectral lags. Hard-to-soft evolution of the spectrum produces positive spectral lags while soft-to-hard evolution would lead to negative lags.

Regardless of its physical origin, the spectral lags show some interesting correlations with other measured parameters. Based on six GRBs with known redshifts, Norris, Marani & Bonnell (2000) found an anti-correlation between the spectral lag and the isotropic peak luminosity ($L_{\rm iso}$). Further evidence for this correlation was provided by many others (Norris 2002; Gehrels et al. 2006; Schaefer 2007; Hakkila et al. 2008). More recently Ukwatta et al. (2011) using 43 Swift

long bursts with known redshifts showed that spectral lag and $L_{\rm iso}$ exhibit a higher degree of correlation in the GRB source frame. Many authors have provided possible explanations of the physical cause of lag luminosity relation. Observed spectral lags, as well as peak luminosity, naturally have a strong dependence on the Doppler factor of the outflow (a function of the Lorentz factor and the direction of motion with respect to the observer). If indeed the Doppler factor is the dominant parameter among GRBs, then a relation between spectral lags or variability and luminosity is expected (Salmonson & Galama 2002). Salmonson (2000) on the other hand argues that the anti-correlation is due to the variations in the line-of-sight velocity of various GRBs. Ioka & Nakamura (2001) suggest that the relation is a result of variations of the off-axis angle when viewing a narrow jet. Alternatively, Schaefer (2004) invokes a rapid radiation cooling effect to explain the correlation.

It has been shown that short GRBs have either small or negligible lags (Norris & Bonnell 2006; Zhang et al. 2006). The average spectral lag as measured for 32 short duration GRBs detected by GBM lies in the range ±32 ms (Foley et al. 2011). According to the lag–$L_{\rm iso}$ relation, these small lag values imply that short bursts are highly luminous. However, based on the redshift measurements of their host galaxies it has been shown that short GRBs are generally less luminous than long bursts. Hence short bursts seem to not follow the lag-luminosity relation (Gehrels et al. 2006). The spectral lag has often been used to identify a short burst from the long ones.

An anti-correlation has also been derived between the GRB spectral lag and the jet opening angle (Salmonson & Galama 2002). This relation, when coupled with the above relation between spectral lag and $L_{\rm iso}$ is another manifestation of the anti-correlation between the isotropic luminosity and the jet opening angle, which is the direct consequence of the standard energy reservoir relation (Frail et al. 2001).

Since the GBM has a large energy bandwidth between the NaI and the BGO detectors (8 keV–40 MeV) it has been possible to study the evolution of GRB spectral lags with energy. Such a study led to new discovery that in some GRBs the spectral lag changed sign at higher energies. For example, GRB 090510 shows no significant spectral lag measured between lowest energy light curve (8–20 keV) and higher energy bands up to an average energy of about an MeV and shows a negative lag at a few MeV and beyond. It saturated at constant value of about 250 ms and remained constant there after (Guiriec et al. 2010; Foley et al. 2011). This could be interpreted as due to the differences in the production processes of low and higher energy γ-rays (see Fig. 10).

4.3.3 *GRB light curve decomposition studies*

Most GRB light curves are highly variable with variability time scale significantly smaller than their overall duration. According to the internal shock model (Ricker et al. 2003), the central engine generates relativistic shells with highly non-uniform distribution of Lorentz factors and the pulses are formed by the collision between a rapidly moving shell with a slower shell as mentioned before. Thus in principle the variability of the GRB light curves may directly correspond to the activity of their central engines (Daigne & Mochkovitch 2003; Nakar & Piran

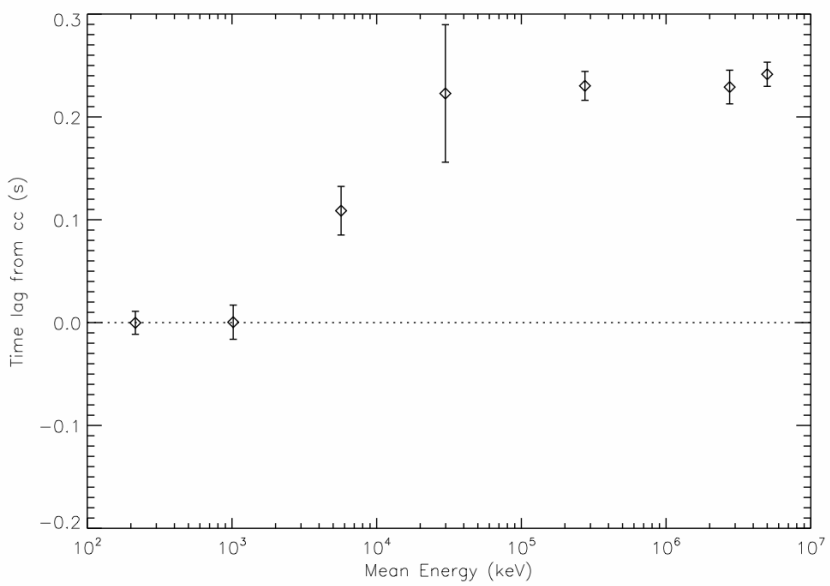

Figure 10. A plot of the spectral lag for the short burst GRB 090510 as a function of mean γ-ray energy. The light curves in the range 8–1000 keV are from the GBM NaI detectors while those in the energy range 1–40 MeV are from the BGO detectors and from the Large Area Telescope (LAT) for the higher energy light curves.

2002). Hence the studies of pulse properties are important to determine whether GRB sources require engines that are long lasting or impulsive (Dermer 2004). Their temporal deconvolution can reveal potential differences in the properties of the central engines in the two populations of GRBs which are believed to originate from the deaths of massive stars (long) and from mergers of compact objects (short). Several authors have studied the deconvolution of GRB light curves into their constituents, and have shown that in general, these are discrete, often overlapping pulses with durations ranging from a few milliseconds to several seconds and almost always asymmetric shapes, with faster rises than decays (Norris et al. 1996; Gupta, Das Gupta & Bhat 2000; Bhat et al. 2011; Hakkila & Preece 2011). These highly varied GRB temporal profiles are suggestive of a stochastic process origin.

In recent years, pulse properties have provided increasingly valuable constraints on the physics responsible for GRB prompt emission. These properties have included (1) temporal asymmetry characterised by longer decay than rise times, (2) hard-to-soft spectral evolution, (3) broadening at lower energies and (4) decreasing pulse height with time since trigger for those GRBs which show hard-to-soft spectral evolution (Norris et al. 1996; Gupta, Das Gupta & Bhat 2002).

Using pulse data contained in individual energy channels, it has been demonstrated that not only the pulses have longer durations at lower energies, but also peak later at the lower energies (Hakkila & Cumbee 2009; Hakkila et al. 2008).

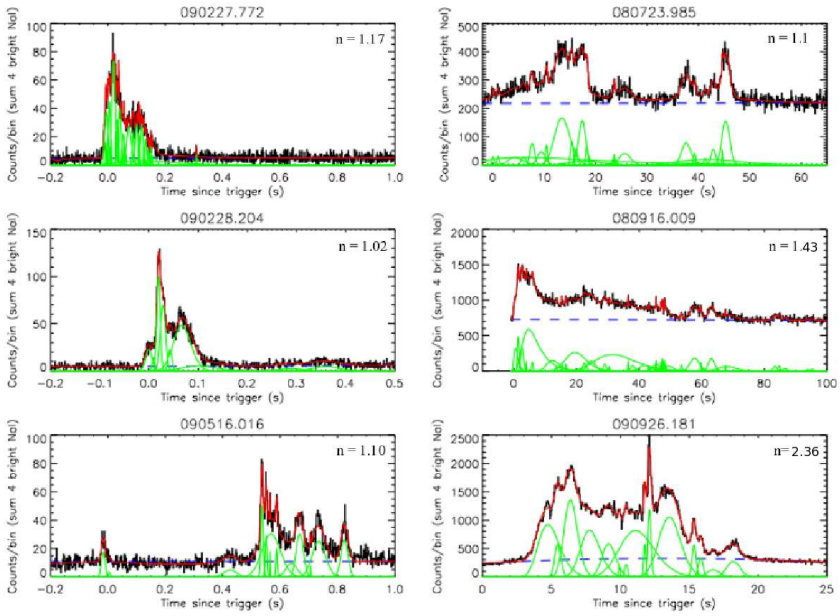

Figure 11. Sample fits to the light curves of 3 short (left column) and 3 long GRBs detected by GBM. Also indicated on the top right of each panel a number equivalent to χ^2 showing the goodness of fit in each case.

Fig. 11 shows a sample of 3 short bursts (left column) and 3 long bursts (right column) whose light curves are deconvolved by fitting log-normal shapes (shown in green at the bottom of each plot) to each pulse in the light curve and then superposed over a quadratic background (shown as dashed line). The resulting fit shown as continuous line in red fits the actual light curve (black histogram) very well. Also shown are the reduced χ^2 values on top right corner in each plot. Bhat et al. (2011) also find fundamental differences in the pulse properties of long and short duration bursts. Fig. 12 (left) shows the distribution of pulse widths and (right) interval between successive pulses for long and short bursts. It is found that both the pulse widths and pulse intervals follow log-normal functions as shown by the fits separately for long and short bursts. The observed separation of the distributions for the two classes of bursts demonstrates that the short burst light curves consist of more closely packed narrower pulses while long burst light curves consist of broader pulses with larger separations between them. These conclusions support internal shock model for GRBs.

4.3.4 *GRB timescales*

According to the internal shock model, the GRB pulses are formed by the collisions among relativistic shells ejected by the central engine with a distribution of Lorentz factors (Γ). A GRB pulse shape depends on three time scales. The hydrodynamic time scale, $t_{\rm dyn}$ (that determines the

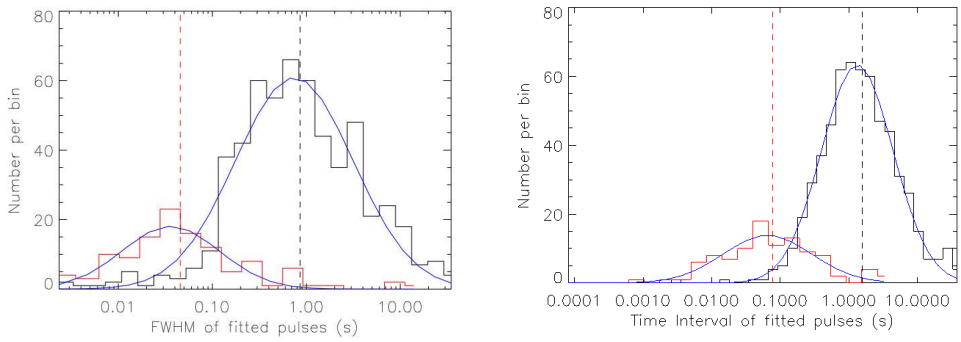

Figure 12. (left) Distributions of the pulse widths (FWHM) for long (histogram shown in black) and short bursts (histogram shown in red). A log-normal function is fitted to each of the distributions. The mean values of FWHM (from the fit) for long and short bursts are 0.89 s and 0.055 s and the standard deviations are 5.2 s and 4.6 s respectively. The vertical dashed lines are the median values of FWHM for each class of GRBs. (right) Distributions of the time intervals between successive pulses (Δt) for long (histogram shown in black) and short (histogram shown in red) bursts. A log-normal function is fitted to each of the distributions. The mean values of Δt (from the fit) for long and short bursts are 1.53 s and 0.076 s and the standard deviations are 3.6 and 5.1 respectively. The vertical dashed lines indicate the median values of the time intervals between successive pulses for each class of GRBs.

pulse rise time), the angular spreading time scale, $t_{\rm ang}$ (that determines the pulse decay time), and the cooling time scale, $t_{\rm rad}$ (which is usually much shorter than the other two and can be ignored) (Kobayashi, Piran & Sari 1997; Katz 1997; Fenimore, Madras & Nayakshin 1996).

In Fig. 13, a spherical shell of width Δ is expanding with a relativistic Lorentz Factor $\Gamma \gg 1$ and emits a photon at radius $r = 0$ from A, at the time of explosion and at $r = R$ from points B, C and D. The time interval between two photons emitted by the shell from points A and B is called the line of sight time, $t_{\rm los}$ and is given by:

$$t_{\rm los} = \frac{R}{2c\Gamma^2}.$$

Similarly the angular time scale, $t_{\rm ang}$, i.e. the interval between the two photons emitted by the shell from points B and C also happens to be equal to $t_{\rm los}$. Similarly the time interval between the two photons emitted from D and B is given by (Sari & Piran 1997)

$$t_{\rm rad} = \frac{\Delta}{2c\Gamma^2}.$$

In the internal dissipation models the burst duration is related to the duration of the engine activity whereas the variability time scale Δt could reflect either the variability of the flow or the irregularities in the radial structure of the shell. The irregularities that it encounters will be spread on a time $t_{\rm ang}$. So $\Delta t \geq t_{\rm ang}$. If the thickness of the shell is Δ in the source rest frame, the rest frame duration of the burst must be longer than Δ/c. In the case of external dissipation models of

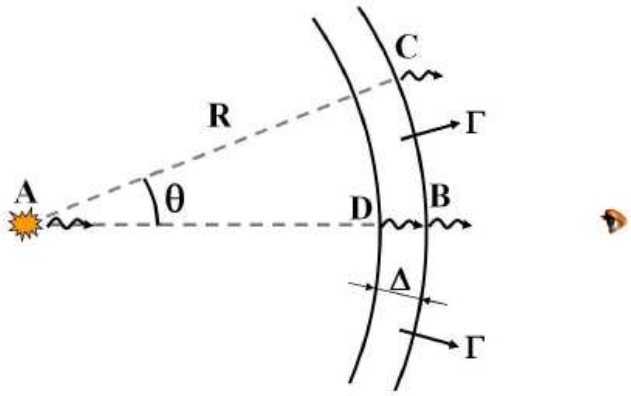

Figure 13. A cartoon of a spherical relativistic shell of width Δ expanding with a Lorentz factor Γ Four photons are emitted as indicated. These photons set three typical time scales. Photon 'A' is emitted from the origin at the time of the explosion. Photons 'B','C' and 'D' are all emitted when the shell front is at radius R. 'B' is emitted from the front of the relativistic shell on the line-of-sight. 'C' is emitted from the front of the shell at an angle θ. 'D' is emitted from the rear of the shell on the line-of-sight.

baryonic outflow energy can be released on an engine dynamical time scale. The duration of the burst in this model is $R_\gamma/10c\Gamma^2$ where R_γ is the radius at which blast wave associated with the fireball becomes radiative (Mitra 1998). The variability time scale in this case is determined by the size of the density fluctuations in the external medium.

Variability time scale is an important parameter which is related to the characteristic timescales of emission process mentioned above. The FWHM of the pulses in a deconvolved light curve may be considered as a measure of variability time scale at any time during the prompt emission. Hence this technique of deconvolving the GRB light curve into pulses enables one to trace the evolution of emission time scale during the prompt emission while a median or a mean FWHM may be considered as a typical variability time scale for a GRB.

The radius in the source frame at which prompt emission takes place can be estimated from the variability time scale as follows:

$$R_{\rm e} \approx \frac{2\gamma_{\rm e}^2 c t_{\rm var}}{1+z}$$

where $t_{\rm var}$ is the GRB light curve variability time scale (Dermer 2004). Using the range of pulse widths required to deconvolve the light curve one can estimate the range of radii where the internal shocks are operating resulting in the observed emission.

4.4 GRB spectral analysis results

In the Fermi Era, GRB prompt emission spectra observed with GBM are still usually adequately fit with the Band function from 8 keV to 40 MeV (Goldstein et al. 2011; Bissaldi et al. 2011) with spectral parameters mostly consistent with what was reported from BATSE data (Goldstein et al., in preparation). However, due to the superior sensitivity of the LAT compared to EGRET, more GRBs have been observed at high energy above 100 MeV. At the current date, GBM detected 800 GRBs (Paciesas et al. 2011) and the LAT detected 28 GRBs (Abdo et al., in preparation). 20 of the LAT GRBs have a significant emission above 100 MeV. The others have a low significance above this energy threshold, but they exhibit a clear signal below (in the 20–100 MeV range).

While in some GRBs, the low energy emission observed in GBM and the high energy emission detected by the LAT start simultaneously, in others the emission onset above 100 MeV is delayed compared to the low energy observed in GBM. However, when started, the structures of the >100 MeV light curves match with the ones observed at lower energy with GBM (see §4.4.1 for more details).

While some joint GBM and LAT spectral fits are consistent with a Band function (Abdo et al. 2009a,b; Abdo et al. 2010a, Abdo et al., in preparation), some exhibit strong deviations, which are well fit with an additional power law in addition to the Band function as reported in González et al. (2003) from CGRO data. Such deviation have been reported several times in both, long (Abdo et al. 2009c; Ackermann et al. 2011) and short Fermi GRBs (Ackermann et al. 2010), and the additional power law usually overpowers the Band function below few tens of keV and above few tens of MeV as seen in figures 14 and 15. This additional power law, with an index value, which usually ranges from -1.5 to -1.9 (harder than the β parameter of the Band function) challenges both leptonic and hadronic models (Asano, Guiriec & Mészáros 2009). For instance, leptonic models such as inverse-Compton (IC) or synchrotron self Compton (SSC) emission can naturally explain the high energy power law. However, they do not support the delayed onset of high energy component nor the low energy power law excess. Hadronic models, through pair cascade or proton synchrotron models (Asano, Guiriec & Mészáros 2009; Razzaque, Mena & Dermer 2009) have difficulties to reproduce the correlated variability at low and high energies. In addition, proton synchrotron emission requires very large magnetic fields. However, they can explain the delayed onset of high energy emission since the time to accelerate protons or to develop cascades is longer than that for electrons. In hadronic models, synchrotron emission from secondary electron-positron pairs produced via photon hadron interactions can naturally explain the power law at low energy. Kumar & Barniol Duran (2009); Ghirlanda, Ghisellini & Nava (2010) also suggested that the additional power law and the delayed high energy emission could originate from an early afterglow and produce by electron-positron synchrotron emission from the external shock. However, the short variability time scale remains a problem.

In some cases, the additional power law does not extend at high energy but can still be fit in addition to the Band function from GBM data alone (Guiriec et al. 2010). For GRB 090926A (Ackermann et al. 2011), a cutoff was required around 1.4 GeV in the additional power law, and this additional component was clearly associated with a very bright peak in the prompt emission

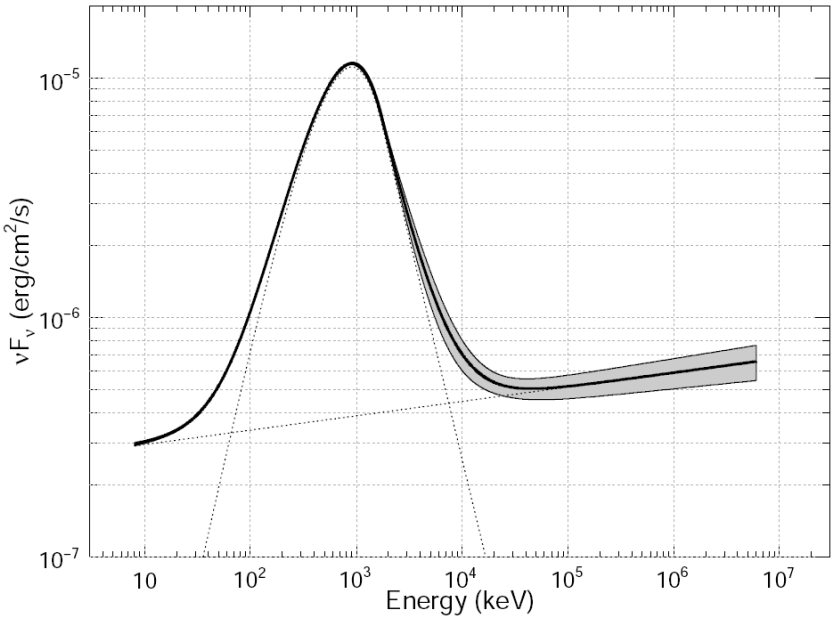

Figure 14. νF_ν spectrum of GRB 090902B as observed with the two instruments on-board Fermi, GBM and LAT. The Band function is insufficient to fit the prompt emission spectrum which requires an additional power law. The additional power law is more intense than the Band function below few tens of keV and above several MeV. The thin dashed lines represents the two components used to fit the spectrum (i.e. Band function and power law), and the thick solid one corresponds to the sum of the two components. The gray butterfly represents the 1 sigma confidence contour taking into account the covariance matrix resulting from the fit.

light curve which dominates the rest of the emission in all energy bands from 8 keV to few tens of MeV (see Fig. 15). Ryde et al. (2011, 2010) reported the fit of bright Fermi GRBs with a combination of a modified black body, called multi colour black body, and an additional power law using fine time interval. More recently, Guiriec et al. (2011) reported for the first time a significant improvement when fitting the time integrated spectrum of GR 100724B with a about 30 keV black body component in addition to the standard Band function (see Fig. 16). The evolution of the thermal and the non thermal components were also followed across the prompt emission using time-resolved spectroscopy and the black body component was consistent with a possible cooling. The simultaneous identification of a thermal component in addition to the traditional non thermal one, is a major step to validate such a result. This black body component was interpreted as the jet photospheric emission, and its characteristics implied that the prompt emission energy released by the central engine could not be of pure internal origin, but that the outflow had to be highly magnetised close to the source. Prompt emission spectra best fit with a combination of a Band function, a black body component and an additional power law have been observed in several Fermi GRBs (Guiriec et al., in preparation).

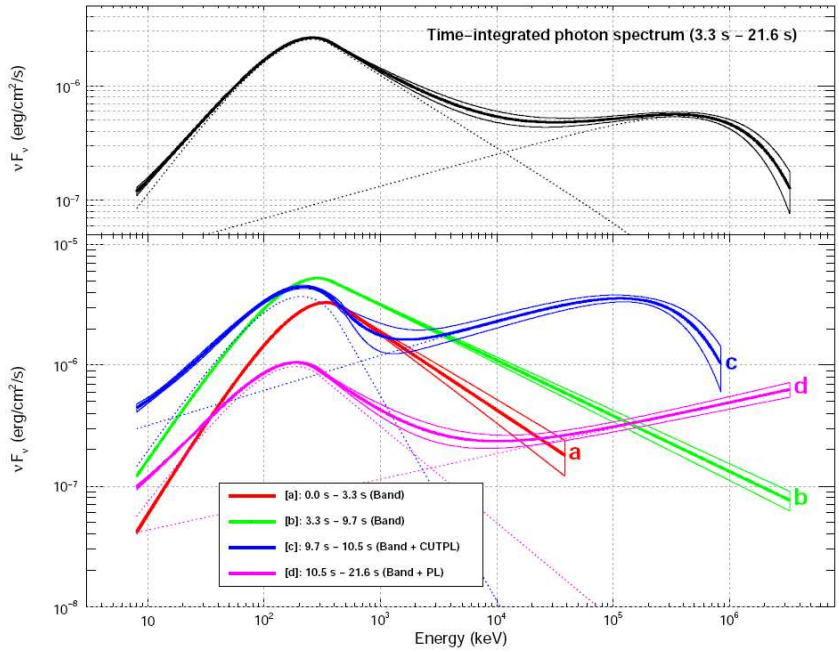

Figure 15. Top panel: νF_ν time integrated spectrum of GRB 090926A. As for GRB 090902B (see Fig. 14), an additional power law is required together with the traditional Band function. However, in this case, a break can be measured in the additional power law around tens of MeV. Bottom panel: Time resolved νF_ν spectra of GRB 090926A. Initially, the prompt emission spectrum is well fit with a single Band function. After few second, the additional power law kicks off. In both the panels, the thin dashed lines represent the two components used to fit the spectrum (i.e. Band or Band function and power law), and the thick solid lines correspond to the sum of the components. The butterflies represent the 1 sigma confidence contour taking into account the covariance matrix resulting from the fits.

Guiriec et al. (2010) reported that the light curves observed at low and high energies in the GBM data where not matching, the highest energy ones exhibiting more numerous sharper structures with $E_{\rm peak}$ tracking these high energy light curves. This suggests the existence of multiple spectral components which are dominating in different region of the spectrum. The high energy emission observed in the LAT lasts usually longer than the prompt emission detected in GBM, and a long lasting high energy emission observed above 100 MeV has been detected up to several ks in some cases (Abdo et al., in preparation).

Estimation of the number of GRBs that the LAT should detect based on extrapolation of the high energy power law when fitting the keV–MeV emission with a Band function are usually too optimistic compared to the real observations. This suggests that the additional power law do not exist in all GRBs, and that the Band function is a too simplistic model to describe the prompt emission spectral shape. Whether a cut off is required around few tens of MeV (Abdo et al., in preparation), which could be explained by emission process or pair creation opacity, or as

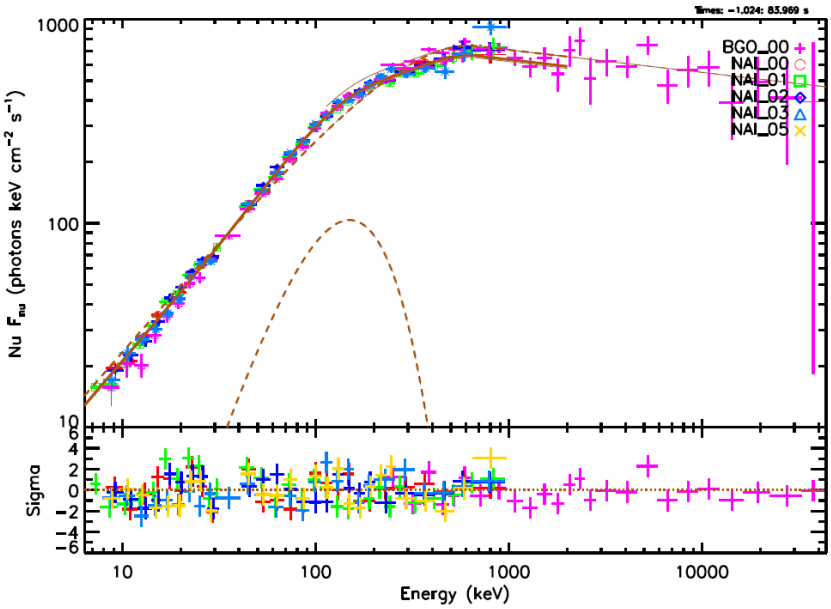

Figure 16. Time-integrated νF_ν spectrum of GRB 100724B as observed with GBM and fit with a Band function and an additional black body component. The thin dashed lines represented the two components used to fit the spectrum (i.e. Band function and black body), and the solid line corresponds to the sum of the two components. The points plotted on the top panel are model dependent and results from the fit of the real count spectrum with a Band function and a black body component. Bottom Panel: residual of the fit when the real count spectrum is fit with a Band function and an additional black body component. A significant black body component is detected, in addition to the traditional Band function. The detection of such a component reinforced the fireball model which predict such a photospheric emission which has never been clearly detected before. The relatively low intensity of the black body component compared to the Band function and the temperature of this component (around $\sim$ 30 keV), imply that the energy reservoir cannot be of purely internal origin, but the outflow has to be highly magnetised close to the source.

reported in Guiriec et al. (2011), the addition of an other component such as a black body to the Band function modify the parameters of the latest making β steeper and more compatible with the number of GRB detected by the LAT. Moreover, the black body component reported in Guiriec et al. (2011) also makes α steeper, and thus, more compatible with synchrotron models.

4.4.1 *Delayed high energy emission*

In the long, bright and hard GRB 080825C triggered by GBM and seen by LAT, high-energy γ ray emission detected by the LAT starts later and persist longer than the lower energy γ ray photons. This is also seen subsequently in the long GRB 080916C, as well as short bursts, GRB 081024B

and GRB 090510C (see LAT catalog). Therefore they appear to be a common feature of bright and hard GRBs seen by both GBM and LAT. The delayed onset of the GRB 080916C LAT pulse, which coincides with the rise of the second peak in the GBM light curve (see Fig. 17), suggests a common origin in a region spatially separated from the first GBM pulse. In the framework of the internal-shock model for the prompt emission of GRBs where intermittent relativistic shells of plasma are ejected by a newly formed black hole and collide to form shocks and accelerate particles, the two emission regions could arise from two different pairs of colliding shells, with variations in physical conditions leading to non-thermal electrons with different spectral hardnesses (Piran 1999; Mészáros 2002). Model based on the proton synchrotron radiation in the prompt phase where the delay is due to acceleration of protons, also is consistent with the high energy spectrum of GRB 080916C (Razzaque, Dermer & Finke 2010).

An alternative explanation for the delayed onset of the LAT emission is that a volume becomes filled with radiation that attenuates the high-energy photons until a later time when the emitting region expands and becomes optically thin (Granot, Cohen-Tanugi & do Couto e Silva 2008). Razzaque, Mészáros & Zhang (2005) have predicted that γ-ray photons typically above

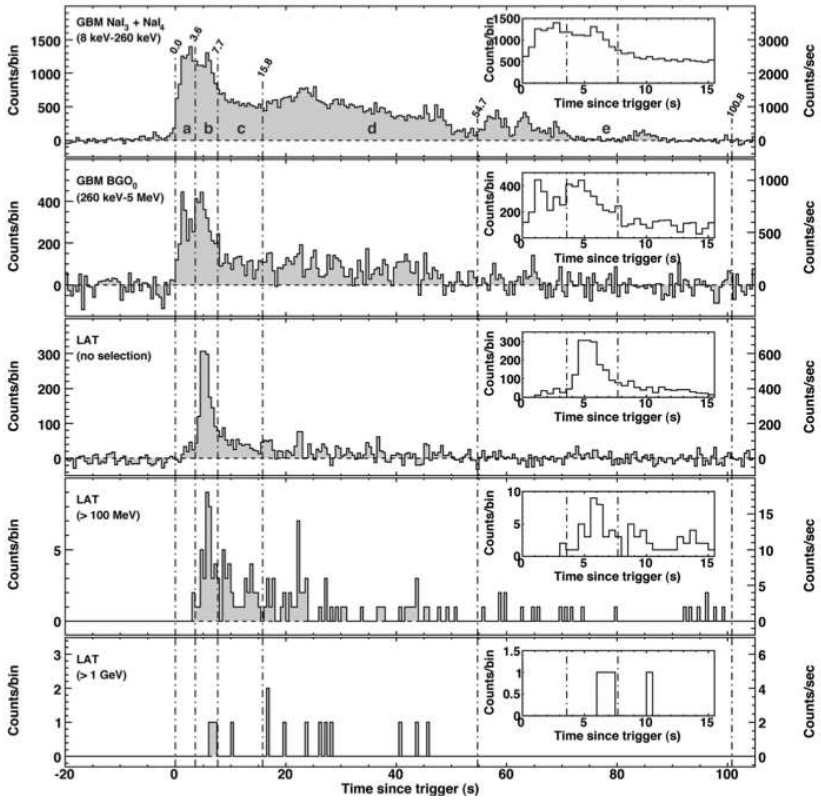

Figure 17. Energy dependent optical depth for γ-rays from the GRBs.

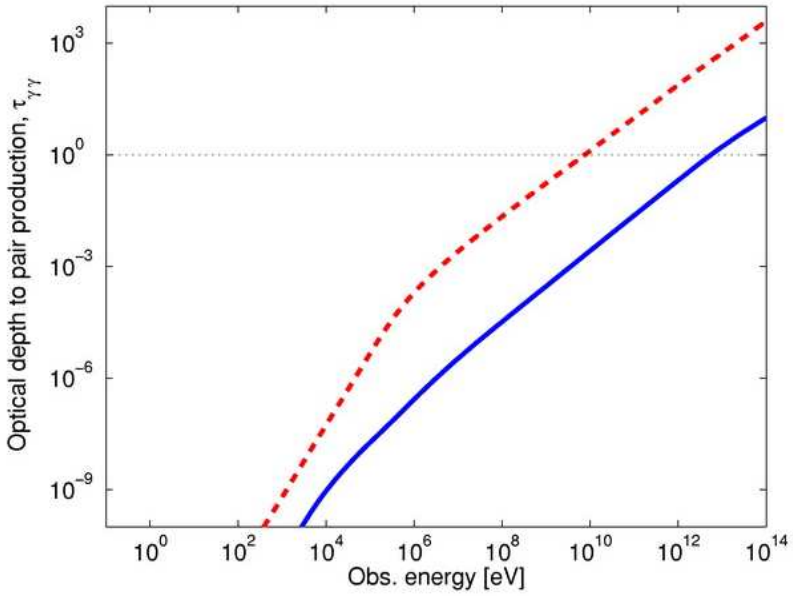

Figure 18. Energy-dependent optical depth to pair production, for the two scenarios. Solid line, Explosion into ISM; dashed line, explosion into a wind.

10–100 GeV will be trapped inside the fireball due to a high opacity of electron-positron pair production with other photons. High energy photons escaping the fireball may interact with cosmic background radiation and provide delayed γ-ray emission. Fig. 18 shows the photon energy dependence of the optical depth inside the fireball (Pe'er & Waxman 2005). A $\gamma\gamma$ pair-production opacity effect would, however, produce a high-energy spectral softening or cutoff, whereas in all cases the combined GBM/LAT data are well fit with simple models by using the Band parameterisation.

For GRB 090510 an electron synchrotron radiation model in the early afterglow has been invoked (Kumar & Barniol Duran 2009; Ghirlanda, Ghisellini & Nava 2010).

5. Inferred results

5.1 Standard candle

During their rather short live time, GRBs are radiating more energy than all the rest of the Universe and could therefore be the farthest objects, which could be possible to detected if they can actually be produced by the first generation of stars and if there is not too much absorption along the line of sight. Similar to type Ia supernovae, if GRBs are standard-like candles, they could sup-

plement the former sample and could be the deepest probes of the cosmos. Lots of efforts have been put into testing hardness-intensity relations in GRB prompt emission. First proposed by Amati et al. (2002) from the BeppoSAX data, the so-called 'Amati relation' relates the observed $E_{\rm peak}$ to the total isotropic energy release. Hence this raised lots of discussion in the community. This relation suggests a correlation between the parameter $E_{\rm peak}$ of the Band function and the total energy radiated during the prompt phase (when corrected for the redshift).

$$E_{\rm peak} \propto E_{\rm iso}^{(0.52\pm0.06)}.$$

The caution on the validity of this relation is the possible instrumental and selection effects. Since the first proposition in 2002, many other derived results have been proposed. Among them the so called Ghirlanda relation is particularly interesting. It states that the collimation-corrected total energy of the bursts, E_γ is well correlated with the source frame $E_{\rm peak}$ as follows:

$$E_{\rm peak}^{\rm obs}(1+z) \propto E_\gamma^{0.7}.$$

The physics of GRBs is far from understood, these relations are purely empirical but survive from one generation of instrument to the other (Amati 2003; Sakamoto et al. 2006). More recently, Goldstein et al. (2010) re-analyzed the full sample of BATSE GRBs, and showed that most of the GRBs violate the limits imposed by the Amati relation, but are consistent with the Ghirlanda relation (Ghirlanda, Ghisellini & Lazzati 2004). Kocevski (2011) very recently showed through the use of a population synthesis code to model the prompt gamma-ray emission from GRBs that a combination of instrumental sensitivity and the cosmological nature of an astrophysical population can artificially produce a strong correlation between observed parameters like the Amati relation.

5.2 Extra-galactic background light

The Extra-galactic Background Light (EBL) is a cosmic diffuse Infra-red (IR)-Optical-Ultraviolet (UV) radiation field produced by the first generation of stars and its reprocessing by the dust in the interstellar medium. The EBL is difficult to study directly because of the intense foreground and galactic emission. However, it is possible to constrain indirectly the EBL by studying its effect on high energy gamma ray emission. In fact, photons with energy above $\sim$ 10 GeV can interact with such a low energy photon field via electron–positron pair production during their propagation from sources at cosmological distances. This will result in a spectral break in the observed spectrum from high energy sources like the Blazars and GRBs which are ideal candidates to study EBL. Thus it is possible to test the density of the EBL photon field by studying its opacity to high energy photons. Study of EBL as a function of the redshift could lead to information on galaxy evolution and star formation in the early Universe. The highest energy photons observed with Fermi, such as the 33.4 GeV photon from GRB 090902B at a redshift of $z = 1.82$, do not support the 'fast evolution' and the 'baseline' models because they predict optical depths of $\tau_{\gamma\gamma} = 7.7$ and 5.8 respectively which is too thick to support the observation (Stecker, Malkan & Scully 2006). Similarly EBL models predicting a greater opacity of the Universe to

high energy γ-rays, in the GeV–TeV, energy range are in disagreement with the observations of Blazars (Stecker, Malkan & Scully 2006, 2007). Results on the measurement of the opacity of the Universe with Fermi are reported in Abdo et al. (2009c, 2010b).

5.3 Lorentz invariance violation

While special relativity assumes that there is no fundamental length-scale associated with Lorentz invariance, some quantum gravity models predict a fundamental length scale (called the Planck scale $l_{\rm Planck} \approx 1.62\times10^{-33}$ cm or $E_{\rm Planck} \approx M_{\rm Planck}c^2 \approx 1.22\times10^{19}$ GeV) at which quantum effects are expected to strongly affect the nature of space-time. This implies that the Lorentz invariance may break at or near the Planck scale. Some quantum gravity models predict a possible test of such a violation is to measure an energy-dependence of the speed of light. To detect such an effect, photons have to propagate very large distances to make possible the measurement of any time delay between photons of various energies emitted at the same time from the source. GRBs are explosive events at cosmological distances, emitting photons over a very large energy range. Although the emission mechanisms involved in GRBs are still not completely understood, it is generally accepted that low and high energy photons are emitted simultaneously from the same emission region and that no known delay can be attributed to any source related emission effects, which is a strong hypothesis that could impact the validity of the results. Any delay between low and high energy photons in the observer frame could then be attributed to photon propagation effects. Most of the models predicting a Lorentz invariance violation conclude that the high energy photons should be delayed with respect to low energy photons, but the opposite could happen as well. The arrival time delay (i.e. lag), Δt, between low and high energy photons, $E_{\rm l}$ and $E_{\rm h}$ respectively, emitted simultaneously and at the same location, is given by (Amelino-Camelia et al. 1998)

$$\Delta t = \xi \left(\frac{E_{\rm h} - E_{\rm l}}{M_{\rm Planck}c^2} \right) \frac{L}{c}$$

(using only linear terms in the dispersion relation) where ξ is a model-dependent factor of the order of unity and L the distance to the source.

All quantum gravity models do not agree on the degree of possible violation. With Fermi, due to its unprecedented energy bandwidth, first order and possibly second order effect could be measured. Abdo et al. (2009a) using GRB 090510 determined lower limits on the quantum gravity mass scale. The technique described previously was applied assuming standard cosmology of a flat expanding Universe with the following parameters $\Omega_M = 0.27$, $\Omega_\Lambda = 0.73$ and $H_0 = 71$ km s^{-1}Mpc^{-1}. Very conservative constraints were provided considering the lag as the duration between the onset of the burst at low energy and the arrival time of the highest energy photons. In the case of the long GRB 080916C, the highest energy photon is a 13 GeV arriving 16.5 s after the GRB onset and for the short GRB 090510, a 31 GeV photon was observed by the LAT 0.83 s after the GBM trigger time. The strongest constraint was obtained for GRB 090510 with $E_{\rm LIV} \geq 1.19E_{\rm Planck}$. Even stronger constraints were obtained using less conservative but

still reasonable assumptions, by associating after-trigger low energy pulses with the high energy photons.

Until now, no significant energy dependence of the speed of light was reported from the Fermi data, which currently provides the best lower limits. This strongly disfavours the quantum gravity models predicting that the granularity of the space-time at Planck scale should lead to a linear dependence of the speed of light with the energy.

6. Future prospects

6.1 VHE and UHE Gamma-rays from GRB Sources

The terrestrial atmosphere provides nearly 28 radiation lengths of shielding to celestial γ-rays. Ground based telescopes like the Imaging Atmospheric Čerenkov Telescopes (IACTs) for very high energy (VHE) γ-ray astronomy and the Extensive Air Shower (EAS) arrays for PeV γ-ray astronomy use the atmosphere itself as the detector of γ-rays. These experiments exploit the characteristics of the secondaries of the electromagnetic cascade initiated by the γ-rays.

IACTs such as MAGIC, VERITAS and HESS, which are still operational and water Čerenkov detectors such as MILAGRO, whose activity stopped in 2008, looked for and are still looking for a possible VHE γ ray signal in the GeV/TeV regime coming from GRBs. More recently MAGIC (Garczarczyk et al. 2010), VERITAS (Galante et al. 2009) and HESS (Aharonian et al. 2009) come online. Until now, only upper limits have been reported for a few tens of GRBs. MAGIC, with a low energy threshold ($\sim$ 25 GeV) and the fastest repointing capabilities is currently the most powerful of these instruments for a quick follow up of the VHE counterpart in GRBs in response to alerts from other instruments provided through GCN. However, MAGIC cannot repoint faster than a few tens of seconds, which is usually too long to catch the prompt emission from the burst. While IACTs suffer from a handicap of low duty cycles and limited field of views, water Čerenkov detectors or the EAS arrays have a full sky coverage and can operate during day and night with no limitation with the Moon's phase. MILAGRITO, a prototype version of MILAGRO, reported a possible VHE γ ray signal in coincidence with GRB 970417A, which triggered BATSE (Atkins et al. 2000). However, MILAGRO, a much more sensitive instrument, unfortunately did not find such a detection (Atkins et al. 2005).

Even though IACTs and water Čerenkov detectors have not succeeded in detecting a VHE γ-ray signal from the GRBs they were only a small number of GRBs. MAGIC energy threshold overlaps with the LAT energy band and hence could have detected the 33 GeV photon observed by the LAT during the prompt emission of GRB090902B (Abdo et al. 2009c). In addition, this photon was detected about 80 s after the GBM trigger time, which is encouraging since MAGIC could have repointed to the burst location during this time. If this burst were to have triggered Swift or LAT and provided a precise location through the GCN system the chances could have been still higher. Future generation IACTs, like the Čerenkov Telescope Array (CTA) (Bouvier et al. 2011), and the future water Čerenkov detector like the High-Altitude Water Čerenkov Observatory (HAWC), if operating simultaneously with Fermi, should be able to undertake the

challenge of detecting VHE γ-ray emission from GRBs. Such a detection will have a major impact on GRB physics. The high energy cutoff, if any, could tell us about the emission process operating at the GRB sources, the acceleration mechanism of the radiating particles, the outflow Lorentz factor as well as the Extra-galactic Background Light (EBL) responsible for VHE extinction (Abdo et al. 2010b).

6.2 Radio emission from GRB sources

A conducting fireball expanding at relativistic speed into an ambient magnetic field generates a rapidly changing electric current which emits coherent electromagnetic radiation at radio frequencies. The critical frequency (upper limit of the emission) strongly depends on the Lorentz factor of the expansion. The radio detection will enable us to estimate the density and structure of the circumstellar material and, by inference, the evolution of the presupernova stellar wind, and reveal the last stages of stellar evolution before explosion. The radio emission can best be explained as the interaction of a mildly relativistic ($\Gamma \sim 1.6$) shock with a dense pre-explosion stellar wind-established circumstellar medium that is highly structured both azimuthally, in clumps or filaments, and radially, with observed density enhancements.

Over the past several years the afterglow of γ-ray bursters has occasionally been detected in the radio (see Chandra & Frail 2011 (this issue) for a comprehensive review on radio afterglow observations from GRBs), as well in other wavelengths. It is possible to model the gross properties of the radio and optical/infrared emission from the half-dozen GRBs with extensive radio observations. From this it is concluded that at least some members of the 'slow-soft' class of GRBs can be attributed to the explosion of a massive star in a dense, highly structured circumstellar medium that was presumably established by the pre-explosion stellar system.

The coherent radio emission is practically simultaneous with the GRB except for the reduced propagation speed of the radio waves by interstellar dispersion. However delayed radio emissions have been detected in the case of GRB 990123 (Kulkarni et al. 1999) which has been interpreted as due to reverse shock. The source of this radio emission could be attributed to incoherent synchrotron radiation of shockwave produced electrons (Paczynski & Rhoads 1993).

Ideally an all sky monitor in the radio frequency range would be an ideal instrument since unknown delays due to dispersion measure as well as intrinsic delays due to the emission process. One such possible detector would be the upcoming LOw Frequency ARray (LOFAR) array which has a sensitivity at low frequencies ($\leq$ 250 MHz) better than the currently operating radio telescopes like the Very Large Array (VLA), Westerbork Synthesis Radio Telescope (WSRT) and Giant Meterwave Radio Telescope (GMRT) array, by more than an order of magnitude.

In addition the Square Kilometer Array (SKA) will be a revolutionary radio telescope with about one square kilometre of collecting area, giving 50 times the sensitivity and 10,000 times the survey speed of the best current day telescopes with a wide bandwidth of frequency range from 70 MHz to 10 GHz. It is expected to become fully operational by 2024. We would certainly expect breakthroughs when these future projects become fully operational.

6.3 Neutrinos from GRBs

Detection of high energy neutrinos from GRBs would test the shock acceleration mechanism and the suggestion that GRBs are the sources of ultra-high energy protons, since $\geq 10^{14}$ eV neutrino production requires 10^{16} eV protons. The dependence of even higher energy neutrino (10^{17} eV) flux on the fireball environment implies that the detection of high energy neutrinos would also provide constraints on the GRB progenitors. Furthermore, it has recently been pointed out that if GRBs originate from core-collapse of massive stars, then a burst of $\geq$ 5 TeV neutrinos may be produced by photo-meson interaction while the jet propagates through the envelope with TeV fluence implying 0.1–10 neutrino events per individual collapse in a 1 km^3 neutrino telescope. It is argued that GRBs have the potential to produce the particle energies (up to 10^{21} eV) and the energy budget (10^{44} erg yr^{-1}Mpc^{-3}) to accommodate the spectrum of the highest energy cosmic rays (see §2.8 for more details). Detection of neutrinos is the only unambiguous way to establish that GRBs accelerate protons.

Detection of neutrinos from GRBs could be used to test the simultaneity of neutrino and photon arrival to an accuracy of $\sim$ 1 s checking the assumption of special relativity that photons and neutrinos have the same limiting speed, especially in view of the recent results from the OPERA experiment at Gran Sasso (Adam et al. 2011).

Hence it is important to search for neutrino emission from GRBs. Is the predicted flux detectable by the existing neutrino telescopes? Waxman & Bachall (1997) show that a large fraction, $\geq$ 10% of the fireball energy is expected to be converted by photo-meson production to a burst of $\sim 10^{14}$ eV neutrinos. As a result we would expect to see several tens of events in a year in a typical neutrino detector of area 2 km^2. This rate is comparable to the background expected from atmospheric neutrinos. However one could easily detect a burst of neutrinos temporally and directionally coincident with the γ-rays from the GRB. The predicted neutrino flux also implies a detection of $\sim$ 10 neutrino induced muon events per year in a planned 1 km^3 Čerenkov neutrino detectors, correlated in time and direction with GRBs. There are several systematic searches for neutrino emission strongly time correlated with GRB signals (Alvarez-Muniz, Halzen & Hooper 2000) produced in a Waxman–Bachall fireball (Waxman & Bachall 1997) as well as model independent searches for neutrinos in a range of energies and emission times with no apparent success (Blaufuss, Meagher & Whitehorn 2011; Presani 2011; Vieregg et al. 2011). Perhaps this lack of success may be understandable if the neutrinos travel with super-luminal velocities (Autiero, Migliozzi & Russo 2011).

The future neutrino detector has the potential to answer some of these critical questions.

6.4 Gravitational waves from GRBs

As predicted in Einstein's General Theory of Relativity, gravitational waves are disturbances in the curvature of spacetime caused by the motions of matter. A promising source of gravitational

waves is the coalescence of compact binary systems, events which are now believed to be the origin of short GRBs because such mergers are asymmetric. In addition, short GRBs are generally closer than long GRBs. Further GRBs provide a convenient time stamp to identify coincident signals from the gravitational wave detectors which are not directional. Sensitivities of some of the upcoming gravitational wave detectors mentioned below are sufficient to allow some possibility for the detection of astrophysical sources, including gravitational wave signals associated with GRBs and SGRs. Propagating at (or near) the speed of light, gravitational waves pass straight through matter, their strength weakens proportionally to the distance travelled from the source. A gravitational wave arriving on Earth will alternately stretch and shrink distances, though on an incredibly small scale – by a factor of 10^{-21} for very strong sources. Gravitational wave astronomy could expand our knowledge of the cosmos dramatically. For example, gravitational waves, though weakening with distance, are thought to be unchanged by any material they pass through and, therefore, should carry signals unaltered across the vast reaches of space. By comparison, electromagnetic radiation tends to be modified by intervening matter. The remarkable thing about a black hole when simulated on a computer is that no matter how it forms or is perturbed, whether by infalling matter, by gravitational waves, or via a collision with another object (including a second black hole), it will 'ring' with a unique frequency known as its natural mode of vibration. It's this unique wave signature that will allow scientists to know if they've really detected a black hole. The signal will tell how big the black hole is and how fast it's spinning. The γ-rays and the afterglow emission of GRBs are thought to be produced at distances from the central engine where the plasma has become optically thin, $r \geq 10^{13}$ cm, which is much larger than the Schwarzschild radius of a stellar mass black hole (or of a neutron star). Hence we have only very indirect information about the inner parts of the central engine where the energy is generated. However, in any stellar progenitor model of GRB one expects that gravitational waves should be emitted from the immediate neighbourhood of the central engine which is known to house a black hole. Gravitational waves emitted from the progenitor itself, would carry more direct information on the properties of the central engine. Therefore, it is of interest to study the gravitational wave emission from GRB associated with specific progenitors.

Existence of a shallow decay phase in the early X-ray afterglows of γ-ray bursts is a common feature. It is possible that this is connected to the formation of a highly magnetised millisecond pulsar, pumping energy into the fireball on timescales longer than the prompt emission. In this scenario, the nascent neutron star could undergo a secular bar-mode instability, leading to gravitational wave losses which would affect the neutron star spin-down. In this case, nearby γ-ray bursts with isotropic energies of the order of 10^{50} erg would produce a detectable gravitational wave signal emitted in association with an observed X-ray light-curve plateau, over relatively long timescales of minutes to about an hour. The peak amplitude of the gravitational wave signal would be delayed with respect to the γ-ray burst trigger, offering gravitational wave interferometers such as the advanced LIGO and Virgo the challenging possibility of catching its signature on the fly (Corsi & Mészáros 2009).

Gravitational waves if detected from well-localised, spiralling in compact-object binaries, like the progenitors of short GRBs, can measure absolute source distances with high accuracy. When coupled with an independent determination of redshift through an electromagnetic counter-

part, these standard sirens can provide an excellent probe of the expansion history of the Universe and eventually the dark energy equation of state parameter w (Dalal et al. 2006).

Hence the ground based gravitation wave detector network consisting of Laser Interferometer Gravitational-Wave Observatory (LIGO), LIGO-II (a planned upgrade of LIGO with tenfold increase in sensitivity), Virgo (Italian and French collaboration for the realization of an interferometric gravitational wave detector which is about to be fully commissioned), and AIGO are vital to realize some the potentials of this technique. LIGO–VIRGO network will become operational in 2015 at the completion of the latest upgrades. Prime candidates for generating detectable radiation are binary black holes whose constituents each have masses of 10–50 $M_{\odot}$. In addition there are several gravitational wave detector arrays planned for the future. Australian Consortium for Interferometric Gravitational wave Astronomy (ACIGA), plans at undertaking research and development aimed at improving the performance of present laser interferometric gravitational wave detectors through advanced designs to ultimate limits set by mechanics, quantum mechanics, lasers and optics. The Einstein Telescope (ET) aims at realization of the conceptual design of a future European third generation gravitational wave detector. In fact the evolution of the current (first generation) gravitational wave detectors is well defined: after the current upgrade to the so-called enhanced level, the detectors will evolve toward their second generation: the advanced Virgo and LIGO detectors.

There are several searches conducted already for gravitational wave signal coincident with GRBs with no clear success (Abbott et al. 2008; Acernese et al. 2008; Alexander 2008). With the commissioning of more advanced detectors there is potential for achieving breakthroughs in the field of Gravitational Wave Astronomy (see Dhurandhar 2011).

Acknowledgements

SG was supported by an appointment to the NASA Postdoctoral Program at the Goddard Space Flight Center, administered by Oak Ridge Associated Universities through a contract with NASA.

References

Abbott B., et al., 2008, ApJ, 681, 1419
Abdo A. A., et al., 2009a, Science, 323, 1688
Abdo A. A., et al., 2009c, ApJ, 706, L138
Abdo A. A., et al., 2009b, ApJ, 707, 580
Abdo A. A., et al., 2010a, ApJ, 712, 558
Abdo A. A., et al., 2010b, ApJ, 723, 1082
Acernese F., et al., 2008, Classical and Quantum Gravity, 25, 225001
Ackermann M., et al., 2011, ApJ, 729, 114
Ackermann M., et al., 2010, ApJ, 716, 1178
Adam T., et al., 2011, arXiv:1109.4897 [hep-ph]
Aharonian F., et al., 2009, A&A, 495, 505

Alexander D., 2008, in Gamma-ray bursts 2007, eds, Galassi M., Palmer D., Fenimore E., AIP Conf. Proc., 1000, 284
Alvarez-Muniz J., Halzen F., Hooper D. W., 2000, Phys. Rev. D62, 093015
Amati L., 2003, Chinese Journal of Astronomy and Astrophysics Supplement, 3, 455
Amati L., et al., 2002, A&A, 390, 81
Amelino-Camelia G., Ellis J., Mavromatos N.E., Nanopoulos D. V., Sarkar S., 1998, Nature, 393, 763
Aptekar R. L., et al., 1995, Space Science Reviews, 71, 265
Asano K., Guiriec S., Mészáros P., 2009, ApJ, 705, L191
Atkins R., et al., 2000, ApJ, 533, L119
Atkins R., et al., 2005, ApJ, 630, 996
Atwood W. B., et al., 2009, ApJ, 697, 1071
Autiero D., Migliozzi P., Russo A., 2011, arXiv:1109.5378 [hep-ph]
Band D., et al., 1993, ApJ, 413, 281
Bednarz J., Ostrowski M., 1998, Phys. Rev. Lett., 80, 3911
Bhat P. N., Fishman G. J., Meegan C. A., Wilson R. B., Brock M. N., Paciesas W. S., 1992, Nature, 359, 217.
Bhat P. N., Fishman G. J., Meegan C. A., Wilson R. B., Kouveliotou C., Paciesas W. S., Pendleton G. N., Schaefer B. E., 1994, ApJ, 426, 604
Bhat P. N., et al., 2011, ApJ, 741, in press, arXiv:1109.4064 [astro-ph]
Bissaldi E., et al., 2011, ApJ, 733, 97
Blaufuss E., Meagher K., Whitehorn N., 2011, in Gamma Ray Bursts 2010, eds McEnery J.E., Racusin J.L., Gehrels N., AIP Conf. Proc., 1358, 351
Bloom J. S., et al., 2006, ApJ, 638, 354
Bloom J. S., Djorgovski S. G., Kulkarni S. R., Frail D. A., 1998, ApJ, 507, L25
Bonnell J. T., Norris J. P., Nemiroff R. J., Scargle J. D., 1997, ApJ, 490, 79
Bouvier A., 2010, Ph.D. Thesis, arXiv:1012.0558 [astro-ph]
Bouvier A., Gilmore R., Connaughton V., Otte N., Primack J.R., Williams D.A., 2011, arXiv:1109.5680 [astro-ph.HE]
Briggs M. S., et al., 1999, ApJ, 524, 82
Cabrera J. I., Firmani C., Avila-Reese V., Ghirlanda G., Ghisellini G., Nava L., 2007, MNRAS, 382, 342
Cavallo G., Rees M. J., 1978, MNRAS, 183, 359
Chandra P., Frail D.A., 2011, BASI, 39, 451
Chen L., Lou Y-Q., Wu M., Qu J-L., Jia S-M., Yang X-J., 2005, ApJ, 619, 983
Cline T. L., et al., 2003, in Gamma-Ray Burst and Afterglow Astronomy 2001, eds Ricker G.R., Vanderspek R.K., AIP Conf. Proc., 662, 143
Corsi A., Mészáros P., 2009, ApJ, 702, 1171
Costa E., et al., 1997, Nature, 387, 783
Crider A., et al., 1997, ApJ, 479, L39
Cucchiara A., Levan A. J., Fox D. B., 2011, ApJ, 736, 7
Daigne F., Mochkovitch R., 1998, MNRAS, 296, 275
Daigne F., Mochkovitch R., 2003, MNRAS, 587, 592.
Dalal N., Holz D. E., Hughes S. A., Jain B., 2006, Phys. Rev. D, 74, id. 063006

Davidson R., Bhat P. N., Li G., 2011, in Gamma Ray Bursts 2010, eds McEnery J.E., Racusin J.L., Gehrels N., AIP Conf. Proc., 1358, 17
Dermer C. D., 1998, ApJ, 501, L157
Dermer C. D., 2002, ApJ, 574, 65
Dermer C. D., 2004, ApJ, 614, 284
Dermer C. D., Mitman K. E., 1999, ApJ, 513, L5
Dhurandhar S.V., 2011, BASI, 39, 181
Djorgovski S. G., et al., 2003, Proc. of the SPIE, 4834, 238
Fenimore E., Madras C. D., Nayakshin, S., 1996, ApJ, 473, 998
Fishman G. J., Meegan C. A., 1995, ARA&A, 33, 415
Fishman G. J., et al., 1994, ApJS, 92, 229
Foley S., Bhat P. N., Gruber D., McBreen S., Tierney D., Greiner J., 2011, in Gamma Ray Bursts 2010, eds McEnery J.E., Racusin J.L., Gehrels N., AIP Conf. Proc., 1358, 183
Ford L. A., et al., 1995, ApJ, 439, 307
Frail D. A., et al., 2001, ApJ, 562, L55
Frail D. A., Kulkarni S. R., Berger E., Wieringa M. H., 2003, AJ, 125, 2299
Frail D. A., Metzger B. D., Berger E., Kulkarni S.R., Yost S.A., 2004, ApJ, 600, 828
Galante N., for the VERITAS Collaboration, 2009, arXiv:0907.4997 [astro-ph.HE]
Garczarczyk M., et al., 2010, in Deciphering the Ancient Universe with Gamma-Ray Bursts, eds, Kawai N., Nagataki S., AIP Conf. Proc., 1279, 312
Gehrels N., 1997, Nuovo Cimento B Serie, 112, 11
Gehrels N., et al., 2006, Nature, 444, 1044
Ghirlanda G., Celotti A., Ghisellini G., 2003, A&A, 406, 879
Ghirlanda G., Ghisellini G., Lazzati D., 2004, ApJ, 2004, 616, 331
Ghirlanda G., Ghisellini G., Nava L., 2010, A&A, 510, L7
Goldstein A., Preece R.D., Briggs M. S., 2010, ApJ, 721, 1329
Goldstein A., et al., 2011, ApJS, submitted
González M. M., Dingus B. L., Kaneko Y., Preece R. D., Dermer C. D., Briggs M. S., 2003, Nature, 424, 749
Granot J., Cohen-Tanugi J., do Couto e Silva E., 2008, ApJ, 677, 92
Gruber D., et al., 2011, A&A, 531, 20
Guiriec S., et al., 2010, ApJ, 725, 225
Guiriec S., et al., 2011, ApJ, 727, L33
Gupta V., Das Gupta P., Bhat P. N., 2000, in Gamma-ray bursts: 5th Huntsville symposium, eds, Kippen R.M., Fishman G.J., MallozziR.S., AIP Conf. Proc., 526, 215
Gupta V., Das Gupta P., Bhat P. N., 2002, arXiv:astro-ph/0206402
Hakkila J., Preece R. D., 2011, ApJ, 740, 104
Hakkila J., Giblin T.W., Norris J. P., Fragile P. C., Bonnell J. T., 2008, ApJ, 677, L81
Hakkila J., Cumbee R. S., 2009, in Gamma-ray burst: Sixth Huntsville symposium, eds, Meegan C., Kouveliotou C., GehrelsN., AIP Conf. Proc., 1133, 379
Horváth I., 2002, A&A, 392, 791.
Hurley K., et al., 1994, Nature, 372, 652
Ioka K., Nakamura T., 2001, ApJ, 554, L163
Johnson W. N., et al., 1993, ApJS, 86, 693

Katz J. I., 1997, ApJ, 490, 663
Kirk J. G., et al., 2000, ApJ, 542, 235
Kobayashi S., Piran T., Sari R., 1997, ApJ, 490, 92
Kocevski D., Liang E., 2003, ApJ, 594, 385
Kocevski D., 2011, arXiv:1110.6173 [astro-ph.HE]
Kouveliotou C., Meegan C. A., Fishman G. J., Bhat P.N., Briggs M. S., Koshut T. M., Paciesas W. S., Pendleton G. N., 1993, ApJ, 413, L101
Kulkarni S. R., et al., 1999, ApJ, 522, L97
Kumar P., Barniol Duran R., 2009, MNRAS, 400, L75
Li Z., Dai Z. G., Lu T., Song L. M., 2003, ApJ, 599, 380
Litwick Y., Sari R., 2001, ApJ, 555, 540
Lytikov M., Blandford R., 2003, MNRAS, 346, 540
McBreen B., Hurley K. J., Long R., Metcalfe L., 1994, MNRAS, 271, 662
Meegan C. A., et al., 2009, ApJ, 702, 791
Mészáros P., 2002, ARA&A, 40, 137.
Mészáros P., 2006, Reports on Prog. in Phys., 69, 2259
Mészáros P., Rees M. J., 1993, ApJ, 405, 278
Mészáros P., Rees M. J., 2000, ApJ, 530, 292
Mészáros P., Laguna P., Rees M. J., 1993, ApJ, 414, 181
Metzger M. R., Djorgovski S. G., Kulkarni S. R., Steidel C. C., Adelberger K. L., Frail D. A., Costa E., Frontera F., 1997, Nature, 387, 878
Mitra A., 1998, ApJ, 492, 677
Nakar E., 2007, Physics Reports, 442, 166
Nakar E., Piran T., 2002, ApJ, 572, L139
Narayan R., Paczynski B., Piran T., 1992, ApJ, 395, L83
Nolan P. L., et al., 1992, IEEE Trans. on Nucl. Sci., 39, 993
Norris J. P., 2002, ApJ, 579, 386
Norris J. P., Bonnell J. T., 2006, ApJ, 643, 266
Norris J. P., Nemiroff R. J., Bonnell J. T., Scargle J. D., Kouveliotou C., Paciesas W. S., Meegan, C. A., Fishman, G. J., 1996, ApJ, 459, 393.
Norris J. P., Marani G. F., Bonnell J. T., 2000, ApJ, 534, 248
Paciesas W. S., Preece R. D., Briggs M. S. Mallozzi R. S., 2001, ESO Astrophysics Symposia, eds E. Costa, F. Frontera, J. Hjorth. Springer-Verlag, 2001, 13
Paciesas W. S., Briggs M. S., Preece R. D., Mallozzi R. S., 2003, in Gamma-Ray Burst and Afterglow Astronomy, eds Ricker G.R., Vanderspek R.K., AIP Conf. Proc., 662, 248
Paciesas W. S., et al., 2011, ApJS, in press
Paczynski B., Rhoads J., 1993, ApJ, 418, L5
Paczynski B., Xu G., 1994, ApJ, 427, 708
Pe'er A., Waxman E., 2005, ApJ, 633, 1018
Peng Z. Y., Yin Y., Bi X. W., Bao Y. Y., Ma L., 2011, AN, 332, 92
Piran T., 1999, Phys. Rep., 314, 575
Piran T., 2003, Nature, 422, 268
Piro L., et al. 2001, in Gamma-ray bursts in the afterglow era, eds. Costa E., Frontera F., Hjorth J., Springer, Berlin, Heidelberg, p. 415

Preece R. D., Briggs M. S., Mallozzi R. S., Pendleton,G. N., Paciesas W. S., Band, D. L., 1998, ApJ, 506, L23
Preece R. D., Briggs M. S., Mallozzi R. S., Pendleton G. N., Paciesas W. S., Band, D. L., 2000, ApJS, 126, 19
Presani E., 2011, in Gamma Ray Bursts 2010, eds McEnery J.E., Racusin J.L., Gehrels N., AIP Conf. Proc., 1358, 361
Razzaque S., Mészáros P., Zhang B., 2005, J. of Mod. Phys. A, 20, 3163
Razzaque S., Mena O., Dermer C. D., 2009, ApJ, 691, L37
Razzaque S., Dermer C. D., Finke J. D., 2010, Open Astronomy Journal, 3, 150
Rees M. J., Mészáros P., 1992, MNRAS, 258, 41
Rees M. J., Mészáros P., 1994, ApJ, 430, L93
Rees M. J., Mészáros P., 2005, ApJ, 628, 847
Rhoads J., 1999, ApJ 525, 737
Ricker G. R., et al., 2003, in Gamma-Ray Burst and Afterglow Astronomy, eds Ricker G.R., Vanderspek R.K., AIP Conf. Proc., 662, 3
Richardson G., Koshut T., Paciesas W. S., Kouveliotou C., 1996, in Gamma-ray bursts: 3rd Huntsville symposium, eds, Kouveliotou C., Fishman G.J., BriggsM.F., AIP Conf. Proc., 384, 87
Ryan J. M., 1989, Nucl. Phys. B Proc. Suppl., 10, 121
Ryde F., 2004, ApJ, 614, 827
Ryde F., 2005a, ApJ, 625, L95
Ryde F., 2005b, A&A, 429, 869
Ryde F., et al., 2010, ApJ, 709, L172
Ryde F., et al., 2011, MNRAS, 415, 3693
Sakamoto T., et al., 2006, ApJ, 636, L73
Salmonson J. D., 2000, ApJ, 544, L115
Salmonson J. D., Galama T. J., 2002, ApJ, 569, 682
Sari R., Piran T., 1997, ApJ, 485, 270
Sari R., Piran T., 1999, ApJ, 517, L109
Sari R., Mészáros, P., 2000, ApJ, 535, L33
Schaefer B. E., 2004, ApJ, 602, 306
Schaefer B. E., 2007, ApJ, 660, 16
Sommer M., et al., 1994, ApJ, 422, L63
Stecker F. W., Malkan M. A., Scully S. T., 2006, ApJ, 648, 774
Stecker F. W., Malkan M. A., Scully S. T., 2007, ApJ, 658, 1392
Tanvir N. R., et al., 2009, Nature, 461, 1254
Thompson C., 2006, ApJ, 651, 333
Ukwatta T. N., et al., 2011, MNRAS, in press
Urata Y., et al., 2007, ApJ, 668, L95
Vanderspek R., et al., 2004, in Gamma-ray burst symposium, eds, Fenimore E., Galassi M., AIP Conf. Proc., 727, 57
van Eerten H. J., Zhang W., MacFadyen A., 2010, ApJ, 722, 235
van Eerten H. J., Meliani Z., Wijers R. A. M. J., Keppens R., 2011, MNRAS, 410, 2016
van Paradijs J., et al., 1997, Nature, 386, 686

van Paradijs J., Kouveliotou C., Wijers, R. A. M. J., 2000, ARA&A, 38, 379
Vieregg A. G. et al., 2011, ApJ, 736, 50
Vietri M., De Marco D., Guetta D., 2003, ApJ, 736, 50
Virgili F. J., Zhang B., Troja E., O'Brien P., 2009, MNRAS, 392, 91
Waxman E., 1995, Phys. Rev. Lett., 75, 386
Waxman E., 2003, Lect. Notes in Phys. 598, 393
Waxman E., Bachall J., 1997, Phys. Rev. Lett., 78, 2292
Zeh A., Klose S., Kann D. A., 2006, ApJ, 637, 889
Zhang Z., Xie G. Z., Deng J. G., Jin W., 2006, MNRAS, 373, 729
Zhang B., Fan Y. Z., Dyks J., Kobayashi S., Meszaros P., Burrows D. N., Nousek J. A., Gehrels N., 2006, ApJ, 642, 354